JOURNAL OF GEOPHYSICAL RESEARCH, VOL. 106, NO. B10, PAGES 21,859-21,882, OCTOBER 10, 2001

Crustal stress field in southern California and its implications for fault mechanics

Jeanne L. Hardebeck[1] and Egill Hauksson

Seismological Laboratory, California Institute of Technology, Pasadena, California, USA

Abstract. We present a new, high spatial resolution image of stress orientation in southern California based on the inversion of earthquake focal mechanisms. We use this image to study the mechanics of faulting in the plate boundary region. The stress field contains significant spatial heterogeneity, which in some cases appears to be a result of the complexity of faulting and in other cases appears to be a cause. Temporal changes in the stress field are also observed, primarily related to major earthquakes. The observed 15° (±10°) rotation of the stress axes due to the 1992 M7.3 Landers mainshock implies that the deviatoric stress magnitude in the crust is low, of the order of 10 MPa. This suggests that active faults in southern California are weak. The maximum principal stress axis near the San Andreas Fault is often at ~50° to the fault strike, indicating that the shear stress on the fault is comparable to the deviatoric stress. The San Andreas in southern California may therefore be a weak fault in a low-strength crust.

1. Introduction

The boundary between the Pacific and North American plates in southern California is a zone of complex deformation over 100 km wide. The right-lateral, strike-slip San Andreas is the major fault, but there are many other important strike-slip, reverse and normal faults (Figure 1). Knowledge of the forces acting on this system is necessary to understand the mechanics of its deformation. Therefore it is important to determine the state of stress in the crust. Of particular interest is whether the stress field is as spatially complex as the faulting or whether the stress field is relatively homogeneous and the complexity of deformation derives from the heterogeneity of crustal structure.

Numerous borehole stress measurements have been made in southern California at shallow (≤3.5 km) depth [*Hickman et al.*, 1988; *Stock and Healy*, 1988; *Shamir and Zoback*, 1992; *Zoback and Healy*, 1992; *Zoback*, 1992; *Kerkela and Stock*, 1996; *Wilde and Stock*, 1997]. Stress orientations at seismogenic (≤15-25 km) depths have been determined from earthquake focal mechanisms [*Michael*, 1987; *Jones*, 1988; *Hauksson*, 1990; *Hartse et al.*, 1994; *Hauksson*, 1994; *Wyss and Lu*, 1995; *Castillo and Zoback*, 1995; *Zhao et al.*, 1997; *Abers and Gephart*, 1997; *Hardebeck and Hauksson*, 1999]. However, since most of these studies focus on an earthquake sequence or a major fault, the spatial coverage of southern California is incomplete.

The goal of this work is to determine stress orientation at seismogenic depths over the entire southern California plate boundary region using a uniform methodology. Because of the high seismicity rates and dense instrumentation in southern California, there are tens of thousands of well-recorded earthquakes which can be used to infer stress orientation, and most seismically active regions can be studied with a spatial resolution of 5-20 km.

The resulting image of stress orientation can be used to study the mechanics of faulting in southern California. Spatial patterns can indicate whether earthquakes are responding to a heterogeneous or generally homogeneous stress field. Temporal changes in stress orientation provide information about how the stress field evolves through time and how it responds to earthquakes. Stress rotations caused by major earthquakes can also be used to estimate the magnitude of deviatoric stress at seismogenic depths. Stress magnitude and orientation are important parameters in earthquake physics because they control the absolute and relative magnitude of the stresses acting on faults.

2. Data and Method

Our data set consists of ~50,000 earthquakes recorded by the Southern California Seismic Network (SCSN) between January 1, 1981, and December 31, 1999, and during the 1975 Galway Lake and 1979 Homestead Val-

[1]Now at Institute of Geophysics and Planetary Physics, Scripps Institution of Oceanography, University of California, San Diego, La Jolla, California, USA.

Paper number 2001JB000292.
0148-0227/01/2001JB000292$09.00

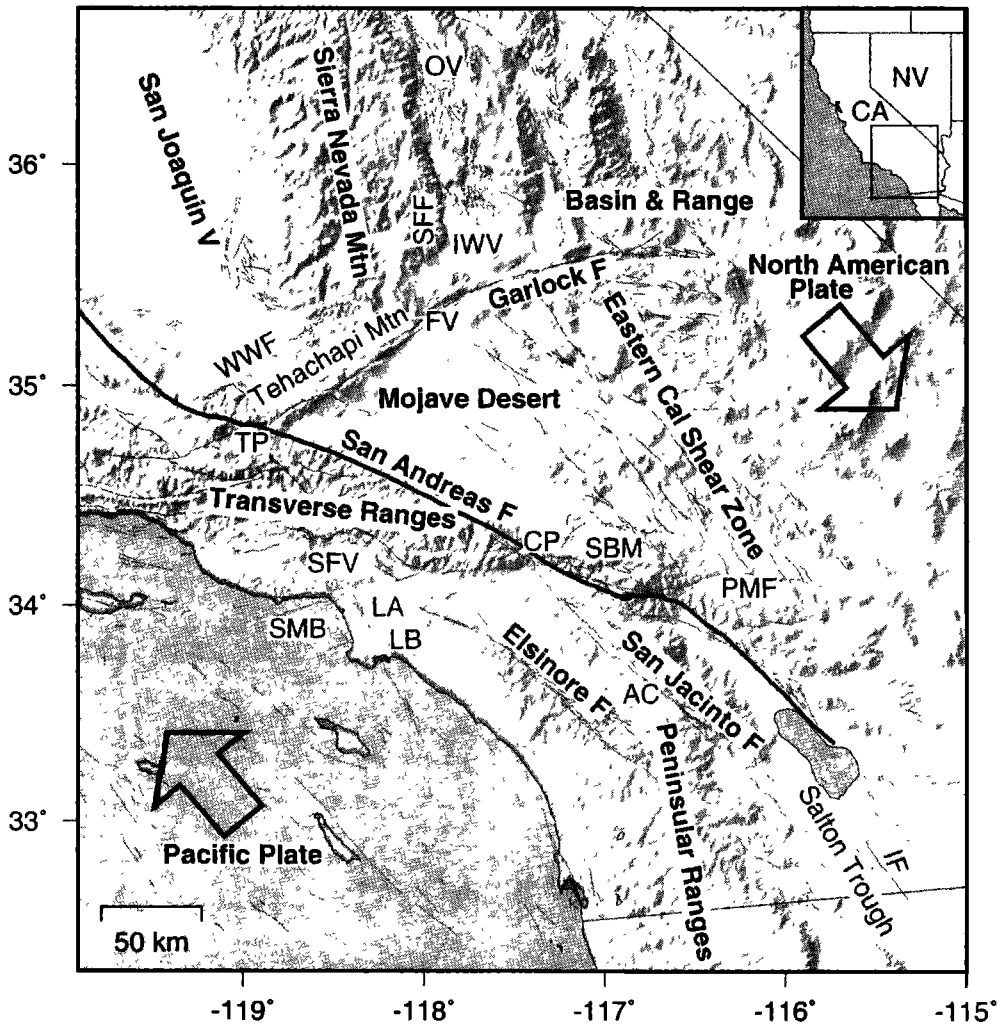

Figure 1. Shaded relief map of southern California. Mapped surface traces of faults shown as thin solid lines [*Jennings*, 1975], the San Andreas Fault as a thick solid line. The arrows indicate the approximate direction of relative motion of the Pacific and North American plates. AC, Anza-Cahuilla region; CP, Cajon Pass; FV, Fremont Valley; IF, Imperial Fault; IWV, Indian Wells Valley; LA, Los Angeles; LB, Long Beach; OV, Owens Valley; PMF, Pinto Mountain Fault; SBM, San Bernardino Mountains; SFF, Sierra Frontal Fault; SFV, San Fernando Valley; SMB, Santa Monica Bay; TP, Tejon Pass; WWF, White Wolf Fault.

ley sequences in the Eastern California Shear Zone. The events were relocated using the three-dimensional seismic velocity model of *Hauksson* [2000]. Focal mechanisms were determined from SCSN first-motion data, using the relocated hypocenters and recomputed take-off angles, with the FPFIT software package [*Reasenberg and Oppenheimer*, 1985]. All events have location uncertainties of $\leq$1 km, $\geq$12 first-motion picks, and a maximum azimuthal gap $\leq$135°.

Inversions of focal mechanisms for stress orientation are performed at points on a three-dimensional grid with 5 km spacing. An inversion includes all events within 5 km of the point if there are $\geq$50 such events. Otherwise, the 50 events closest to the grid point are used. The spatial resolution clearly varies with seismicity rate. We define the 1σ level of spatial uncertainty to be the RMS distance of the events used in the inversion. Results are presented only for locations with spatial uncertainty $\leq$20 km. Most seismically active regions are covered at this level of resolution.

The earthquake focal mechanisms are inverted for stress using the method developed by *Michael* [1984]. The inversion returns the orientation of the three principal stress axes and a measure of their relative magnitude. *Hardebeck and Hauksson* [2001] demonstrate that this inversion method produces accurate stress orientations with reasonable uncertainty estimates.

The inversion of earthquake focal mechanisms for stress orientation relies on two assumptions about the data set: that stress is relatively homogeneous over the spatial and temporal extent of the events and that the focal mechanisms are adequately diverse. The assump-

tion of mechanism diversity can be tested qualitatively by displaying P and T axis distributions. Alternatively, it may be tested quantitatively by calculating a measure of the mechanism diversity, such as the RMS angular difference from the average mechanism. In Appendix A we find that an RMS angular difference of at least ~40°-45° (for focal mechanisms with 10°-20° errors) is required for a reliable stress inversion.

The assumption of homogeneous stress was studied by *Michael* [1991], who found that as long as the magnitude of the uniform part of the stress field is larger than the magnitude of the variable part, an inversion based on the assumption of homogeneous stress will correctly recover the uniform part of the stress tensor. For the inversion method of *Michael* [1984, 1987], an average misfit of the focal mechanisms to the best fit stress tensor of less than ~35°-45° (for focal mechanisms with 10°-20° errors) indicates that this condition is met. Where reliable inversion results can be found, they are understood to represent the uniform part of a stress field in which some heterogeneity may exist.

3. Observations

The orientation of the maximum horizontal stress, σ_H, and the style of faulting are shown in Plate 1 and Plate 2, respectively. The average orientation of σ_H is ~N7°E. However, the observed local direction of σ_H varies greatly, from ~N30°W to ~N45°E (Plate 1). If the orientation of σ_H is not distinguishable from N7°E at the 95% confidence level of the inversion, it is shown in Plate 1 as N7°E. Any observed spatial heterogeneity in stress orientation is therefore statistically significant with respect to the computed uncertainty.

Throughout most of southern California, the intermediate stress axis, σ_2, is closest to vertical, consistent with strike-slip faulting [*Anderson*, 1951]. There are also regions in which σ_1 or σ_3 is closest to vertical, corresponding to the presence of active normal or thrust faults. A variation of the relative magnitude parameter [*Simpson*, 1997] is used to indicate which principal stress is closest to vertical (Plate 2). The deviation of this axis from vertical is generally not statistically significant.

The stress inversion results for most seismically active regions appear to be of good quality. Shown in Plate 3 are four measures of the quality: the spatial resolution; the 1σ uncertainty of the stress orientation, as found by bootstrap resampling [*Michael*, 1987]; the average misfit of the focal mechanisms to the best fit stress tensor; and a measure of the diversity of the focal mechanisms. Most of the study area is covered at ~5-12 km resolution and has a stress orientation uncertainty <12°. The mechanism diversity is generally high, with an RMS angular difference from the mean mechanism of >40°, indicating that there is adequate mechanism diversity for reliable stress inversion. While much of the region shows average focal mechanism misfit <40°, in some areas, there are clusters of higher misfit, indicating that the stress field there is very heterogeneous and that the uniform part of the stress field may not have been found by the inversion.

3.1. Transverse Ranges

Through the Transverse Ranges, which run east-west across the plate boundary region, the San Andreas Fault trends WNW, forming a large-scale constraining bend. In the Transverse Ranges west of Cajon Pass, σ_3 is often vertical, consistent with observed thrust faulting and uplift of the ranges. The orientation of σ_H in the Transverse Ranges is typically ~N7°E, although near Tejon Pass and in the San Bernardino Mountains, σ_H trends NNW, and north of Los Angeles, there is a region of NNE orientation.

In the Cajon Pass region, there is a local σ_1 vertical stress regime. Although the major faults are strike-slip, normal faults have been mapped near Cajon Pass [*Weldon and Springer*, 1988]. *Jones* [1988] also observed this normal faulting regime and attributed the extension to an unstable triple junction where the San Jacinto Fault obliquely joins the San Andreas. The continuation of the observed normal faulting regime to the north and south of Cajon Pass may be an artifact of smearing, as both of these regions have low seismicity rate and low spatial resolution (Plate 3a.)

Stress orientations observed at 3.5 km depth in the Cajon Pass borehole appear to imply left-lateral shear stress on the San Andreas [*Shamir and Zoback*, 1992; *Zoback and Healy*, 1992]. However, we do not observe these left-lateral orientations. A shear wave splitting study indicates that the observed left-lateral stress orientations are local to the upper few kilometers of the borehole site [*Liu et al.*, 1997]. The stress state along the San Andreas changes in both orientation and style of faulting near Cajon Pass, which may result in local stress anomalies such as that observed in the borehole. The geometric complexity of the fault may be responsible for the stress variations near Cajon Pass [*Saucier et al.*, 1992].

In the Transverse Ranges east of Cajon Pass, σ_2 is generally vertical. Although the steep topography of the San Bernardino Mountains implies recent uplift, the observed faulting regime is primarily strike slip. The most recent major earthquake in the San Bernardino Mountains, the M6.2 1992 Big Bear event, was also pure strike-slip [*Hauksson et al.*, 1993]. This suggests that the oblique convergence across the San Bernardino Mountains is partitioned into strike-slip and thrust earthquakes. The thrust faults along the northern face of the mountains strike approximately perpendicular to the σ_H direction, enabling them to fail in thrust even though the stress regime is strike-slip.

3.2. Eastern California Shear Zone

The Eastern California Shear Zone (ECSZ) is a zone of strike-slip faulting east of the San Andreas [*Dokka*

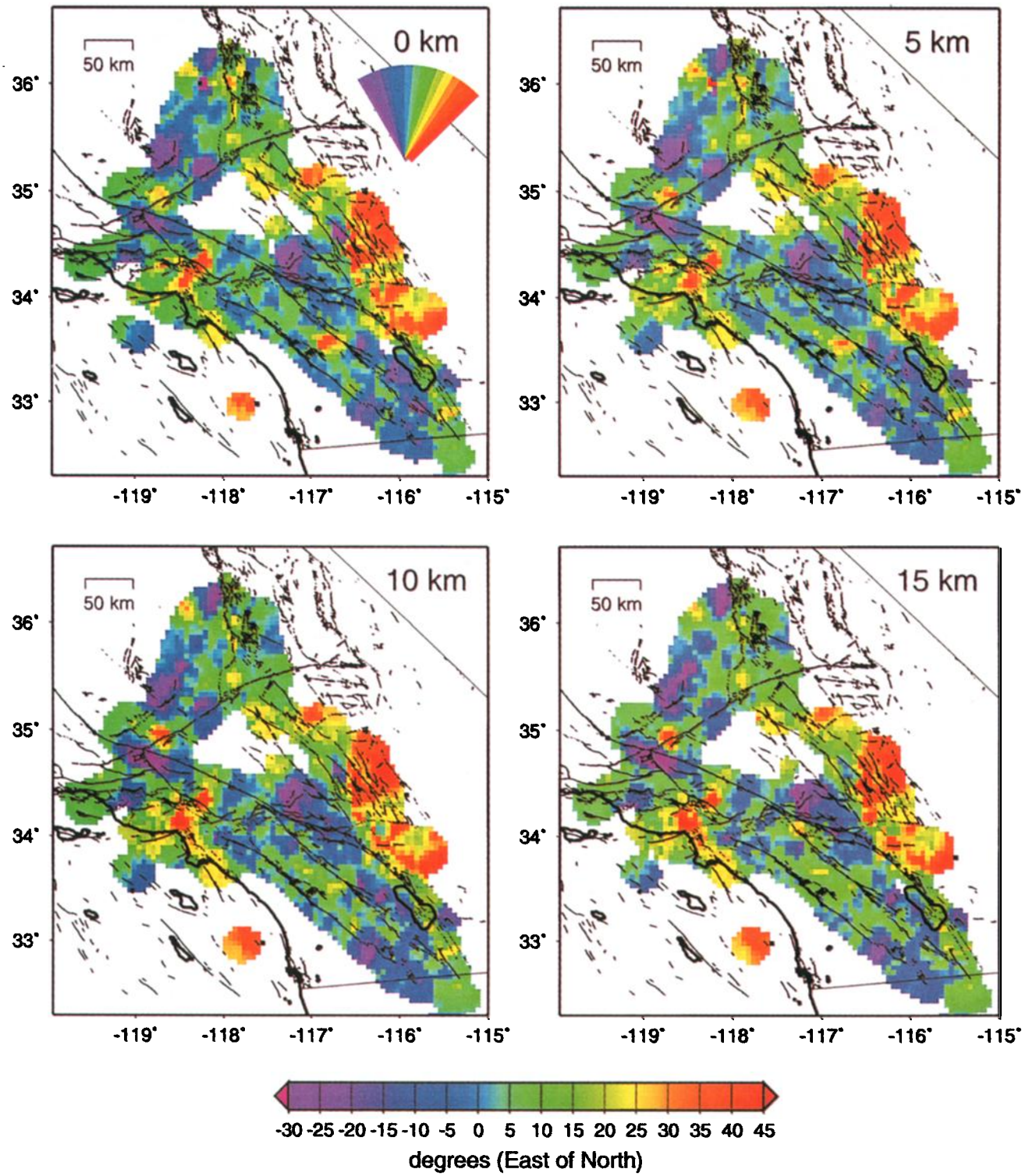

Plate 1. Orientation of the observed maximum horizontal compressive stress, σ_H, at 0, 5, 10, and 15 km depth, measured in degrees clockwise from north. A data set of ~50,000 earthquake focal mechanisms was used to invert for stress orientation. An inversion is performed at each point on a 5-km spaced grid using all earthquakes within 5 km of the point or the 50 events closest to the point, whichever data set is largest. If the orientation of σ_H is indistinguishable form N7°E at the 95% confidence level of the inversion, it is shown as N7°E.

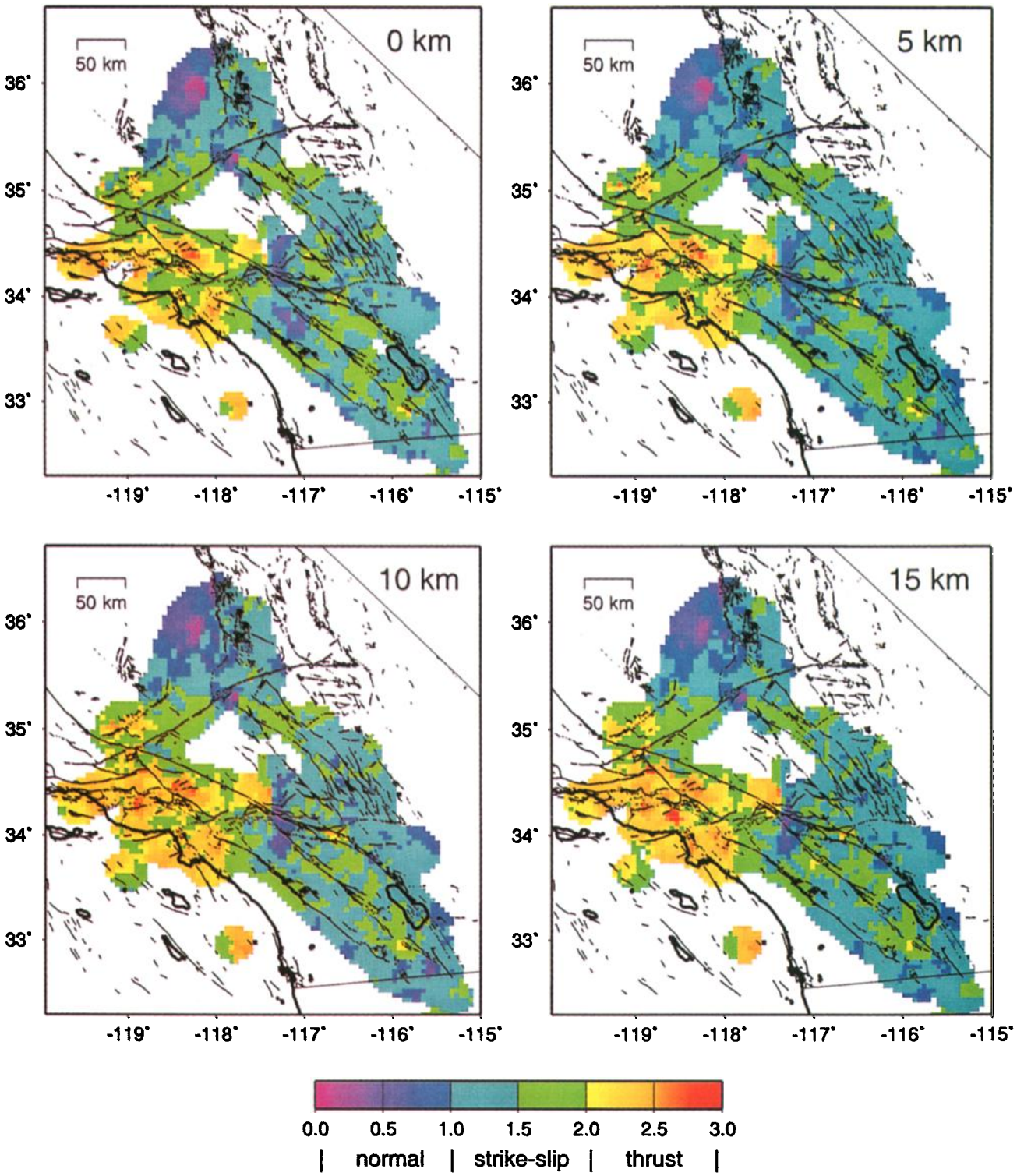

Plate 2. Relative magnitude of the three principal stress axes, A_ϕ, for the same inversions as shown in Plate 1. The parameter A_ϕ is as defined by *Simpson* [1997]. If the maximum principal stress, σ_1, is vertical, corresponding to a normal faulting regime, A_ϕ ranges from 0 to 1. $A_\phi \approx 0$ indicates pure dilatation, $\sigma_2 \approx \sigma_3$; and $A_\phi \approx 1$ indicates a mix of normal and strike-slip faulting, $\sigma_2 \approx \sigma_1$. Similarly, if the minimum principal stress, σ_3, is vertical, corresponding to a thrust faulting regime, A_ϕ ranges from 2 to 3. $A_\phi \approx 3$ indicates pure compression, $\sigma_2 \approx \sigma_1$; and $A_\phi \approx 2$ indicates a mix of thrust and strike-slip faulting, $\sigma_2 \approx \sigma_3$. If σ_2 is vertical, a strike-slip regime, A_ϕ ranges from 1 to 2, depending on whether it is closer to a normal or a thrust faulting regime.

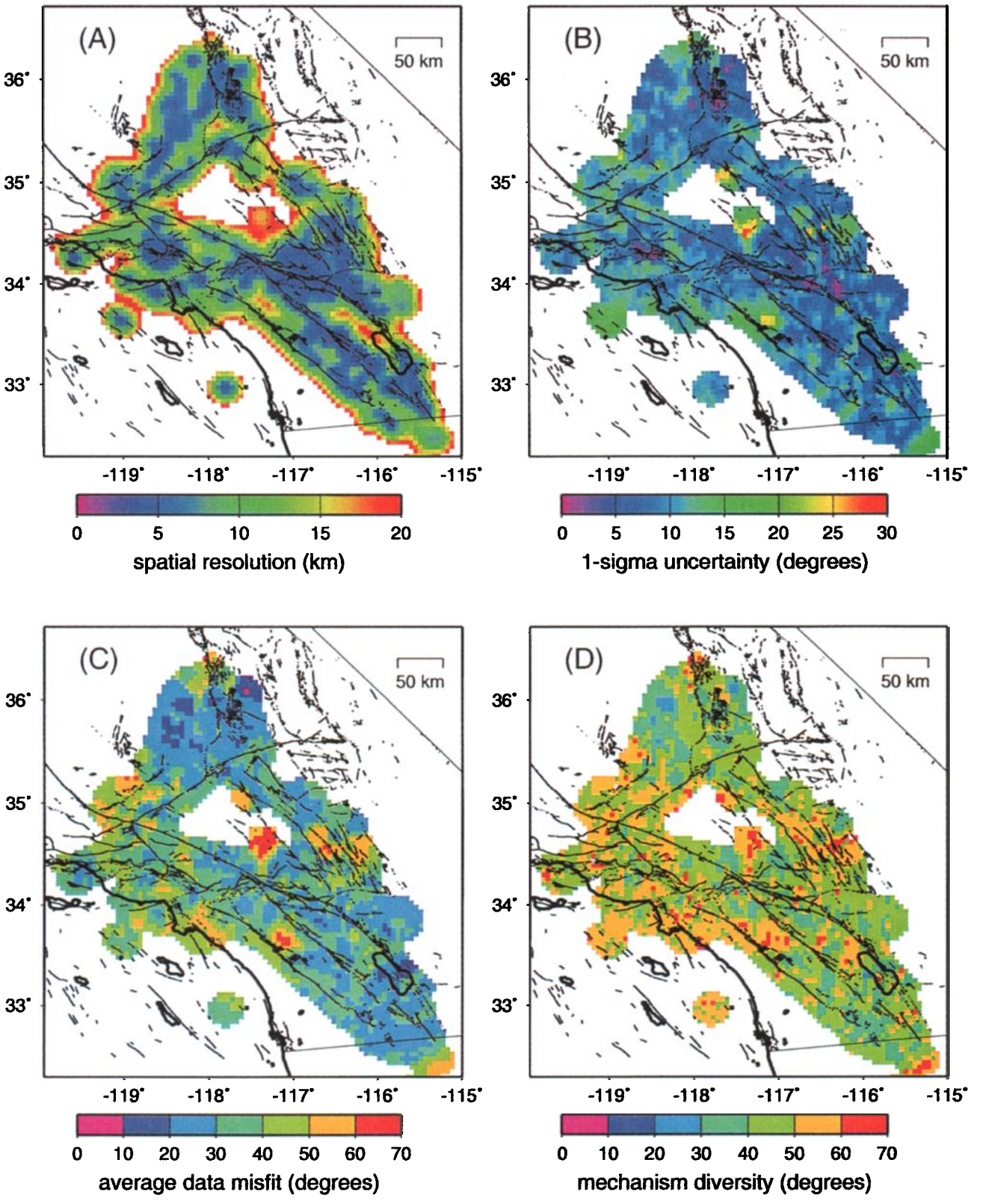

Plate 3. Four measures of the quality of the inversion results shown in Plates 1 and 2, for grid points at 10 km depth. (a) The spatial resolution, defined as the RMS distance from the grid point of earthquakes used in the inversion. (b) The 1σ stress orientation uncertainty, determined using a bootstrap resampling technique. (c) The average misfit of the focal mechanisms used in the inversion to the best fitting stress tensor. The misfit is defined as the angle between the rake direction and the direction of resolved shear stress on the fault plane. An average misfit less than $\sim 40°$ implies a good quality inversion result. (d) The focal mechanism diversity, defined as the RMS angular difference from the average mechanism. A diversity of at least $\sim 40°$ is necessary for a reliable inversion result.

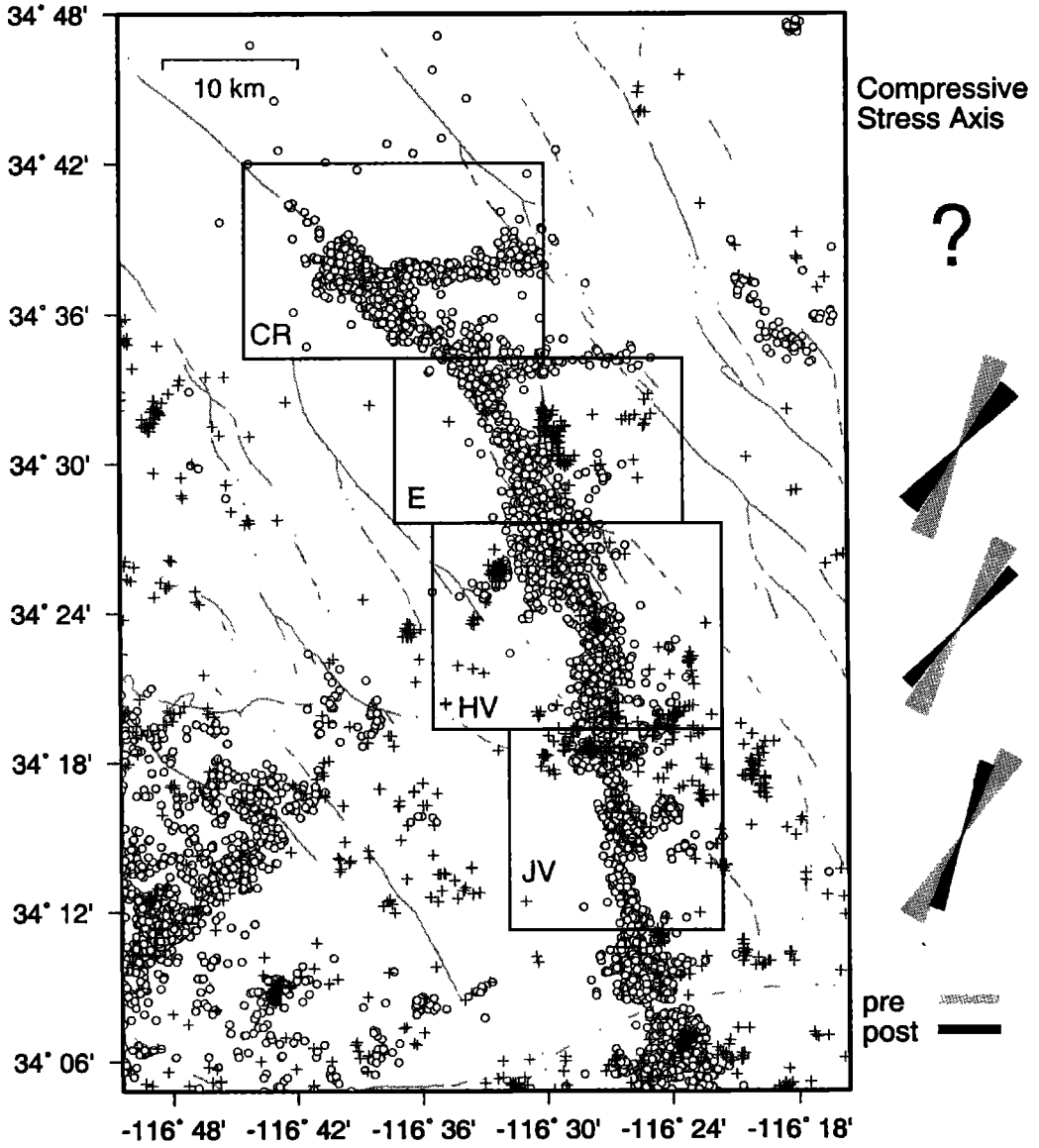

Figure 2. Premainshock and postmainshock seismicity and stress orientation along the 1992 Landers earthquake rupture. The events shown as crosses occurred prior to the Landers mainshock, while those shown as circles occurred after. The four fault segments, Johnson Valley (JV), Homestead Valley (HV), Emerson (E), and Camp Rock (CR), are shown along with boxes indicating the spatial extent of the events used in the stress inversions. To the right, the orientation of σ_H before and after the mainshock. The width of the wedge indicates the 95% confidence region. No results are shown for the Camp Rock segment because there is inadequate premainshock seismicity to perform an inversion, and the average aftershock mechanism misfit along this segment is high, indicating heterogeneous stress.

and Travis, 1990]. The ECSZ south of the Garlock Fault has a distinct stress state, with σ_H oriented N20°-45°E. North of the Garlock Fault, this stress orientation continues only in a narrow zone along the eastern edge of the Sierra Nevada Mountains. The σ_2 axis is vertical throughout most of the ECSZ, although patches of σ_1 vertical stress regime appear.

The 1992 M7.3 Landers earthquake, a right-lateral strike-slip event in the ECSZ [*Sieh et al.*, 1993], altered the stress field in the crust surrounding the rupture (Figure 2 and Table 1, [*Hauksson*, 1994]). Along the northernmost part of the rupture, the average aftershock focal mechanism misfit is high. This indicates that the postmainshock stress field is very heterogeneous, possibly due to complex slip in the Landers earthquake. There is inadequate premainshock seismicity to study the stress field in the area prior to Landers. Along the southern and central rupture, however, there is adequate premainshock and postmainshock seismicity. The average misfit is ~40°, and the mechanism diversity is ~40°-70°, implying that the stress inversion results shown in Figure 2 accurately represent the uniform part of the stress tensor.

The σ_H axis of the uniform part of the stress field

Table 1. Landers Fault Segments

Segment	θ [a]	$\Delta\theta$ [b]	D,[c]m	$\Delta\tau$,[d]MPa	$\Delta\tau/\tau$ [e]	τ,[f]MPa
Johnson Valley	37±13°	-12±9°	2.0±0.5	5.0±1.2	0.63 (0.25-1.0)	7.9 (3.8-25)
Homestead Valley	54±13°	15±9°	3.5±0.5	8.8±1.2	0.67 (0.4-1.0)	13 (7.6-25)
Emerson	63±12°	18±11°	4.0±0.5	10±1.2	0.62 (0.35-0.85)	16 (10-32)

[a]Angle of premainshock σ_H to fault strike; 2σ uncertainty given.
[b]Rotation of the σ_H axis, positive clockwise; 2σ uncertainty given.
[c]Average surface slip, D, estimated from *Sieh et al.* [1993].
[d]The stress drop, $\Delta\tau$, is computed from the definition $\Delta\tau = \mu D/L$, assuming a fault length scale, L, of 12 km (i.e., the rupture broke the entire seismogenic crust) and μ=3x10^{10} N/m^2.
[e]Ratio of stress drop to deviatoric stress, observed from Figure 9; range of acceptable values in parentheses.
[f]Deviatoric stress magnitude; range of acceptable values in parentheses.

along the Emerson and Homestead Valley Faults, in the central part of the rupture, rotated 15°-18° (±10°) clockwise, while the σ_H axis along the Johnson Valley Fault, in the southern part of the rupture, rotated 12° (±9°) counterclockwise. During the 7 years following the mainshock, there is no significant change in stress orientation and no return to the pre-Landers stress state (Figure 3). Unfortunately, it will not be possible to observe whether there is a return to the preevent stress over a longer time period, as the 1999 Hector Mine earthquake occurred ~20 km from the Landers rupture, possibly impacting the stress field in the study region.

The pre-Landers stress state confirms the observation of *Nur et al.* [1993] that along the southern portion of the rupture, where the earthquake nucleated, the mapped faults are poorly oriented for failure, ~70°-80° from σ_H. The southern Landers rupture, however, which cut across the fabric of the mapped faults, is nearly optimal for failure, 37° (±13°) from σ_H. The continuation of the earthquake on the more poorly oriented faults of the northern section may have been controlled by the rupture dynamics.

3.3. Southern Sierra Nevada

The Sierra Nevada Mountains and the San Joaquin Valley to the west form a relatively stable microplate. The stress regime in the southern Sierra Nevada appears to be predominately σ_1 vertical with $\sigma_2 \approx \sigma_3$. This stress state is consistent with a high mountain range in which the stress is primarily controlled by the excess overburden pressure. The western Sierra shows low focal mechanism diversity (Figure 3d), so the stress there may not be well resolved.

Spatial stress variations in the Tehachapi Mountains and the southern San Joaquin Valley may be related to the 1952 M7.7 earthquake on the White Wolf Fault [*Ellsworth*, 1990]. The seismicity in this region divides into a southwestern cloud and a northeastern cluster (Figure 4.) In the southwest, the σ_H orientation is indistinguishable from N7°E, and the style of faulting is predominately thrust. The P and T axis orientations of the individual mechanisms qualitatively support this observation, as most of the P axes trend between N10°W and N10°E, and many of the T axes are subvertical. *Castillo and Zoback* [1995], in contrast, found a N5°W σ_H orientation for the southwestern seismicity and a predominately strike-slip faulting regime. The probable reason for the difference in results is the high stress field heterogeneity in this region, indicated by the high data misfit (Figure 3c.) The stress field is too heterogeneous for the uniform part to be found, and the earthquakes used in the two studies sample this variable stress field differently. In the northeastern region, on the other hand, where the lower data misfit indicates that the uniform part of the stress tensor can be recovered, the two studies are in better agreement. We find a σ_H trend of ~N20°W, while *Castillo and Zoback* [1995] find a trend of N10°W, within the 95% confidence range of our result, and both studies find a strike-slip faulting regime. Spatially-variable slip in the 1952 earthquake may be responsible for the stress field heterogeneity in the southwestern region and the along-strike variability in stress orientation.

The Basin and Range extensional province begins east of the Sierra Nevada. The stress orientations east of the Sierras are primarily strike slip, however, with only a few σ_1 vertical zones. *Bellier and Zoback* [1995] also observed that the stress regime in the western Basin and Range is currently predominately strike-slip. Geodetic data indicate that the slip rate of strike-slip faults striking approximately north in the Indian Wells Valley and southern Owens Valley is >10 times greater than the slip rate of the normal Sierra Frontal fault [*Hearn and Humphreys*, 1998]. The eastern edge of the Sierra Nevada is also a zone of rotated stress, with σ_H oriented ~N20°-45°E. This stress orientation makes the approximately north striking faults well-oriented for strike-slip failure.

3.4. Greater Los Angeles Area

The greater Los Angeles (LA) area is in the southern end of the Transverse Ranges thrust regime. Both σ_2

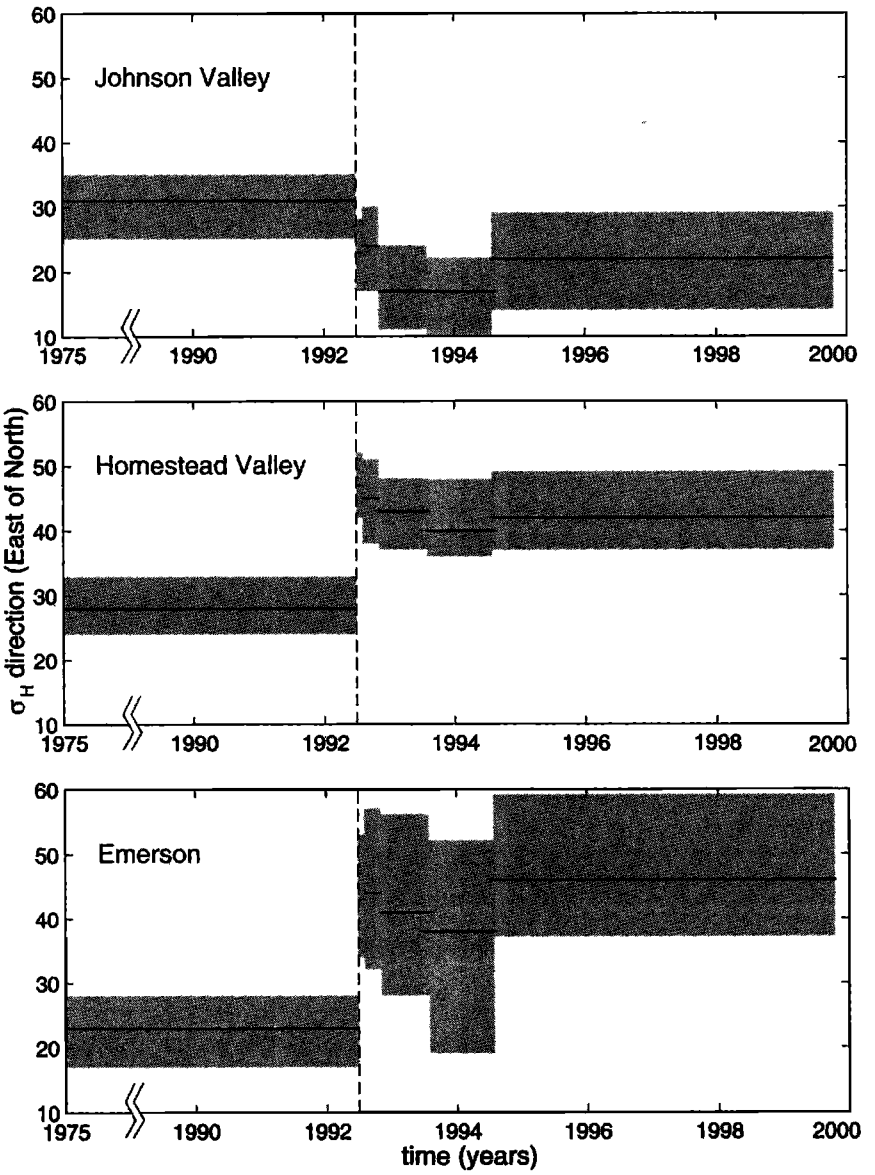

Figure 3. Orientation of the maximum horizontal compressive stress, σ_H, through time in the region of the 1992 Landers earthquake, as determined by inverting earthquakes in three of the boxes shown in Figure 2. The solid line is the orientation of σ_H for the best fitting stress tensor, and the shaded area is the 95% confidence range. Vertical dashed lines indicate the time of the mainshock.

vertical and σ_3 vertical stress states are observed in the LA area, with σ_2 vertical dominating near the surface and σ_3 vertical dominating at depth. *Kerkela and Stock* [1996] observed a similar depth dependence of faulting regime in the San Fernando Valley.

Two recent kinematic models argue that the approximately N-S contraction across the LA area is balanced by approximately E-W extension on conjugate strike-slip faults [*Walls et al.*, 1998] or by thrust faulting and crustal thickening [*Argus et al.*, 1999]. Both models are essentially two-dimensional and assume that the style of faulting at the surface is the same as at depth. The stress field indicates that a three-dimensional model, in which faulting style may vary with depth, would be more realistic.

The σ_H orientation in the LA area is predominately indistinguishable from N7°E. However, there are regions in which σ_H is oriented ~N25°-45°E in the San Fernando Valley, the Long Beach area, Santa Monica Bay, and at depth beneath Los Angeles. Similar spatial variations were observed by *Hauksson* [1990]. The San Fernando Valley rotation corresponds to the locations of the 1971 M6.5 San Fernando [*Ellsworth*, 1990] and 1994 M6.7 Northridge [*Hauksson et al.*, 1995a] earthquakes, while the Long Beach rotation corresponds to the location of the 1933 M6.3 Long Beach earthquake

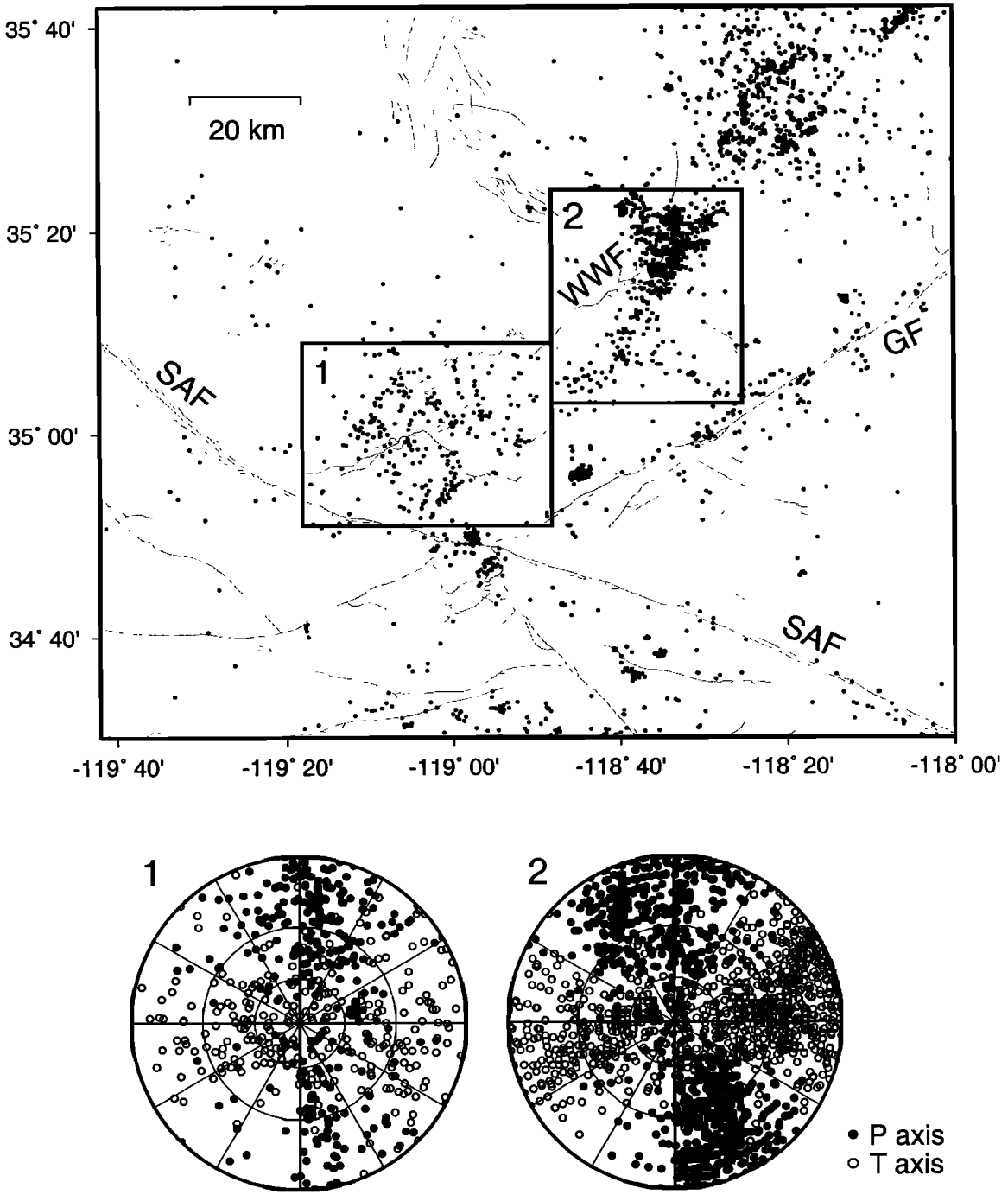

Figure 4. Earthquakes used in the stress inversions in the region of the White Wolf Fault. (top) Seismicity in map view, along with major faults. GF, Garlock Fault; SAF, San Andreas Fault; WWF, While Wolf Fault. (bottom) Lower hemisphere stereographic projections of the P axes (solid circles) and T axes (open circles) of the focal mechanisms of earthquakes occuring within the two boxes shown in the map.

[*Ellsworth*, 1990]. The locations of these events also exhibit high data misfit (Plate 3c), indicating a high level of stress field heterogeneity, perhaps caused by heterogeneous slip in the earthquakes.

The thrust-faulting Northridge event may have altered the stress state in the San Fernando Valley region. *Zhao et al.* [1997], using SCSN polarity data and the stress inversion method of *Horiuchi et al.* [1995], observed a counterclockwise rotation of ~20° at the time of the Northridge earthquake, and a slow return to the original stress orientation. The takeoff angle data used in that study was unavailable, but we obtained a list of the earthquakes (D. Zhao, written communication, 1999) and attempted to reproduce these results.

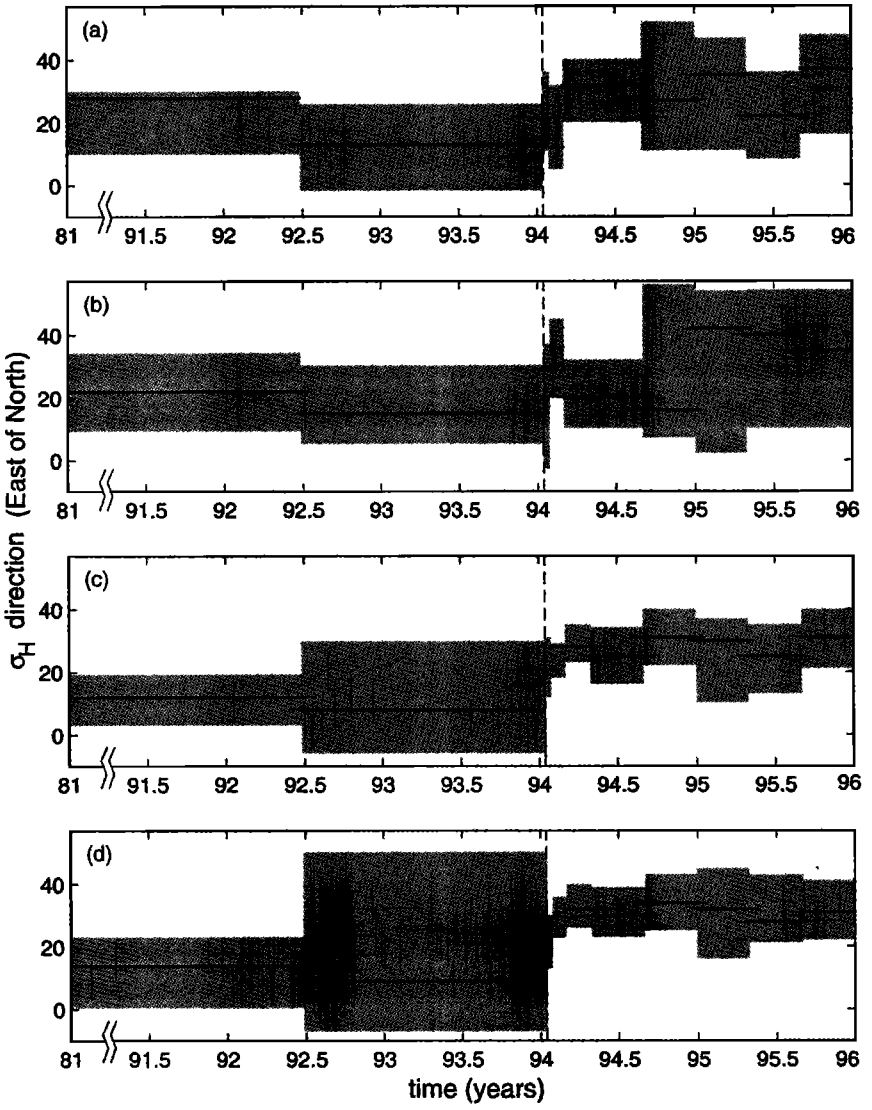

Figure 5. Orientation of the maximum horizontal compressive stress, σ_H, through time in the region of the 1994 Northridge earthquake. The temporal binning is the same as used by *Zhao et al.* [1997]. The solid line is the orientation of σ_H for the best fitting stress tensor, and the shaded area is the 95% confidence range. Vertical dashed lines indicate the time of the mainshock. (a) Results obtained by Y. Sugihara and D. Zhao (written communication, 1999) for an earthquake data set composed of ~90% of the events used by *Zhao et al.* [1997]. First-motion polarities from the SCSN and takeoff angles found using the 3-D seismic velocity model of *Hauksson* [2000] were inverted for stress orientation using the method of *Horiuchi et al.* [1995]. (b) Results obtained by Y. Sugihara and D. Zhao (written communication, 1999) for the same data set with takeoff angles computed from the 3-D seismic velocity model of *Zhao and Kanamori* [1995], using the inversion method of *Horiuchi et al.* [1995]. (c) Results for the same data set as in Figure 5a, inverted using the method of *Michael* [1984, 1987]. (d) Results for the same data set as in Figure 5b, inverted using the method of *Michael* [1984, 1987].

We created a focal mechanism data set from observed SCSN first motion polarities and takeoff angles computed from the seismic velocity model of *Hauksson* [2000]. This set contains ~90% of the events used by *Zhao et al.* [1997]; the other mechanisms were of too poor quality. Y. Sugihara and D. Zhao (written communication, 1999) created a similar data set using takeoff angles computed from the seismic velocity model of *Zhao and Kanamori* [1995]. We inverted both data sets using the inversion method of *Michael* [1984, 1987]. The results suggest a clockwise stress rotation at the time of the mainshock and no return to the premainshock orientation, although the error bounds are large (Figure 5). Y. Sugihara and D. Zhao (written communication, 1999) also inverted the same data sets, using the method of *Horiuchi et al.* [1995], and found the stress

orientations to be unstable and also in poor agreement with the results of *Zhao et al.* [1997].

The inversion results using the method of *Horiuchi et al.* [1995] are unstable with respect to the details of the data set and are not coherent through time. On the other hand, the inversion results using the method of *Michael* [1984, 1987] are stable with respect to the data set and temporally coherent, except at the time of the mainshock. The method of *Michael* [1984, 1987] has also been demonstrated to produce accurate results even for very noisy data [*Hardebeck and Hauksson*, 2001], so it seems more probable that the Northridge earthquake caused a general clockwise, rather than counterclockwise, stress field rotation.

3.5. Peninsular Ranges

The San Jacinto Fault and the Elsinore Fault, two major strike-slip faults which parallel the San Andreas, cut obliquely through the Peninsular Ranges. The stress state is generally strike slip with σ_H oriented ~N7°E. There are a number of patches where the σ_H axis is oriented ~N10°-30°W, most of which are elongate in the direction of the fault trend. There is also an anomalous region near Anza where σ_H trends ~N30°E, also observed by *Hartse et al.* [1994], corresponding to the Cahuilla cluster of shallow seismicity.

The Salton Trough, to the east of the Peninsular Range, is currently experiencing deformation at very high strain rates [*Johnson et al.*, 1994]. The stress regime is primarily strike slip, consistent with the geodetic observations and with the major strike-slip earthquakes on the Imperial Fault in 1940 and 1979 [*King and Thatcher*, 1998]. There is a zone of σ_1 vertical stress to the east of the Salton Sea, corresponding to an area of pure dilatation observed geodetically by *Johnson et al.* [1994].

3.6. Western Mojave Desert

The western Mojave Desert is a stable block with very few earthquakes, so the stress field cannot be constrained from focal mechanism inversion. *Richards-Dinger and Shearer* [2000] concluded that the few observed events in the western Mojave block are primarily quarry blasts, as they occur in clusters and only during the day. Not surprisingly, inversion results based on these data are of poor quality, with very high average misfit (Figure 3c).

4. Discussion

4.1. Spatial Stress Field Heterogeneity

The high-resolution stress orientation images presented here demonstrate that the stress field in southern California is spatially heterogeneous. All of the spatial stress variations discussed above are statistically significant at the 95% confidence level of the stress inversion technique. The length scale of the observed heterogeneity varies from tens to hundreds of kilometers. Smaller-scale variations may also exist, as the inversion results represent the uniform part of the stress field on a 5-20 km length scale. Stress orientations observed in the Cajon Pass borehole, for example, vary by up to 45° over ~1 km [*Shamir and Zoback*, 1992].

Some of the stress orientation complexity is related to differences between the major geologic provinces. The distinct stress states of some regions are easily understood in terms of their tectonics. In the western Transverse Ranges, for example, the thrust faulting stress regime is related to convergence across the large-scale constraining bend in the San Andreas Fault. In other regions the reason for a distinct stress state is unclear. In the ECSZ, for instance, σ_H is oriented N20°-45°E, significantly rotated from the average southern California orientation of N7°E.

Additional stress field heterogeneity is related to fault complexity, such as step overs and junctions. For instance, a zone of normal faulting occurs along the Garlock Fault to the southeast of the Sierra Nevada Mountains. This extension is due to a left step in the left-lateral Garlock Fault, where the Fremont Valley is being downdropped. Another example is the normal-faulting regime at the junction of the San Andreas and San Jacinto Faults.

Major earthquakes also appear to contribute to stress field heterogeneity. The large data misfits (Figure 3c) observed in the regions of the 1933 Long Beach, 1952 Kern County (in the southwestern portion), 1971 San Fernando, 1992 Landers (in the northern portion), and 1994 Northridge earthquakes imply that the heterogeneous part of the stress field in these areas is larger than the uniform part. Spatial variability in earthquake slip is a likely cause of this stress heterogeneity.

The heterogeneity of the observed stress field implies that the complex crustal deformation in southern California is not simply the response of a heterogeneous crust to a homogeneous stress field. In some cases, the complexity of faulting may be a result of the heterogeneous stress field. For example, the N20°-45°E trend of σ_H in the ECSZ may be responsible for Landers and other earthquakes rupturing approximately north trending planes [*Nur et al.*, 1993], instead of planes subparallel to the relative plate motion. In other cases, such as fault jogs, stress field heterogeneity appear to be the result of fault complexity. Complex faulting may promote heterogeneous stress, and vice versa.

4.2. Temporal Evolution of the Stress Field

In order to investigate how the stress field may change through time, we invert for stress during four ~5-year time periods: 1981-1985, 1986-1990, 1991-1994, and 1995-1999. The inversions are performed as described above, except only events occurring within the given time period are used.

The distribution of the σ_H orientations appears to change over the 19 years of this study (Figure 6). In 1981-1985 and 1986-1990 the σ_H direction for most of

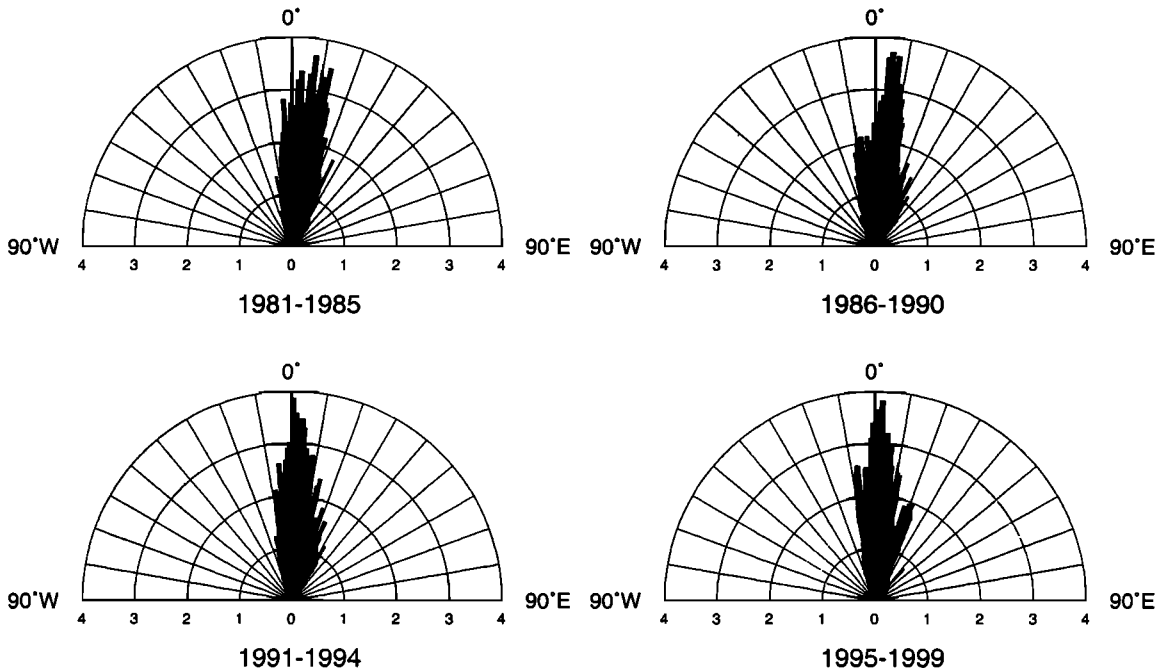

Figure 6. Rose diagrams of σ_H axis orientation during four time intervals. The focal mechanisms of earthquakes occurring during each time interval were inverted using the same technique as in Plate 1. The length of each sector indicates the percent of grid points at which the inversion result falls within a 1°-wide bin.

the grid points trends between due north and N10°E. In 1991-1994 and 1995-1999, σ_H for many points trends between N3°W and N7°E. This suggests a slight counterclockwise rotation of the stress axes since 1981. In the later time periods, there is also a more pronounced peak at ~N20°E. This secondary peak is due to the general clockwise rotations caused by the Landers and Northridge earthquakes and to increased activity in the ECSZ, where σ_H is typically oriented ~N20°E.

The temporal stress change at a given location can be quantified by fitting a constant rotation rate to the observed stress orientations for the four time intervals (Plate 4). Many of the regions which exhibit a high rotation rate, greater than ~1.5°/yr, are in the vicinity of major earthquakes: 1992 Landers, 1994 Northridge, 1987 Elmore Ranch and Superstition Hills [*Wald et al.*, 1990], and 1995 Ridgecrest [*Hauksson et al.*, 1995b]. As stress in the regions of major earthquakes tends to be highly heterogeneous, some of the observed temporal changes may be artifacts of changes in spatial sampling. Other areas that exhibit high rotation rates are at the southern end of the Elsinore Fault, scattered locations near Cajon Pass, along the Garlock Fault near Tejon Pass, and along the San Andreas north of the Salton Sea.

Rotations associated with the tectonic loading of a fault may be difficult to detect. The most that the σ_H axis could rotate would be from ~90° to the fault immediately following a major earthquake to ~45° by the time of the next event. If σ_H rotates ~45° over ~200 years at a constant rate of ~0.2°/yr, the rotation could not be easily detected because it is well below the noise level. If the rotation rate was variable, however, the rotation rate over a ~20-year time interval could be larger and may be detectable. It is therefore possible that the rotations along the San Andreas and Garlock faults may be related to tectonic loading.

4.3. Stress Magnitude and Fault Strength

Major earthquakes appear to have significant impact on stress orientation. Stress rotations and high levels of stress heterogeneity are seen at the locations of the 1933 Long Beach, 1952 Kern County, 1971 San Fernando, 1987 Superstition Hills, 1992 Landers, and 1994 Northridge earthquakes. These perturbations imply that the background deviatoric stress magnitude is low, of the order of earthquake stress drop. If earthquake-induced stress changes were negligible compared to the deviatoric stress, they would not noticeably alter the stress field.

The Landers earthquake appears to have rotated the stress axes in some regions by 15° (±10°) (Figure 2 and Table 1, [*Hauksson*, 1994]). The premainshock and postmainshock seismicity is not collocated, so it is possible that the apparent temporal stress rotation is due to differences in sampling of a region containing spatial variations in stress orientation. However, since the pre-Landers stress state does not show any significant spatial or temporal variation [*Hauksson*, 1994], it is not unreasonable to assume that the premainshock stress

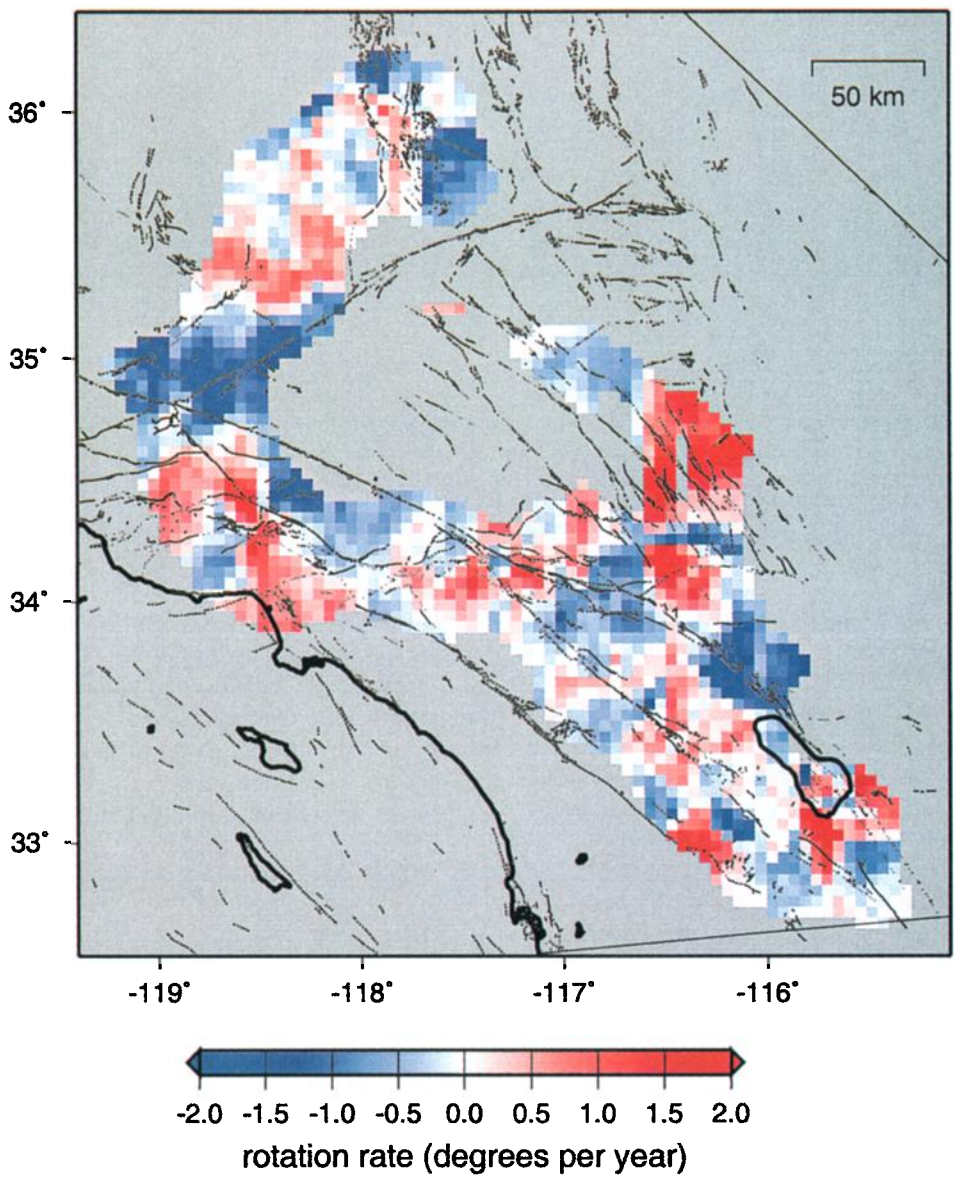

Plate 4. Rotation per year over the duration of the study. The rotation rate at each grid point was found by fitting a least squares linear trend to the inversion results for the four time intervals summarized in Figure 6. Gray indicates there are inadequate data to estimate a rotation rate.

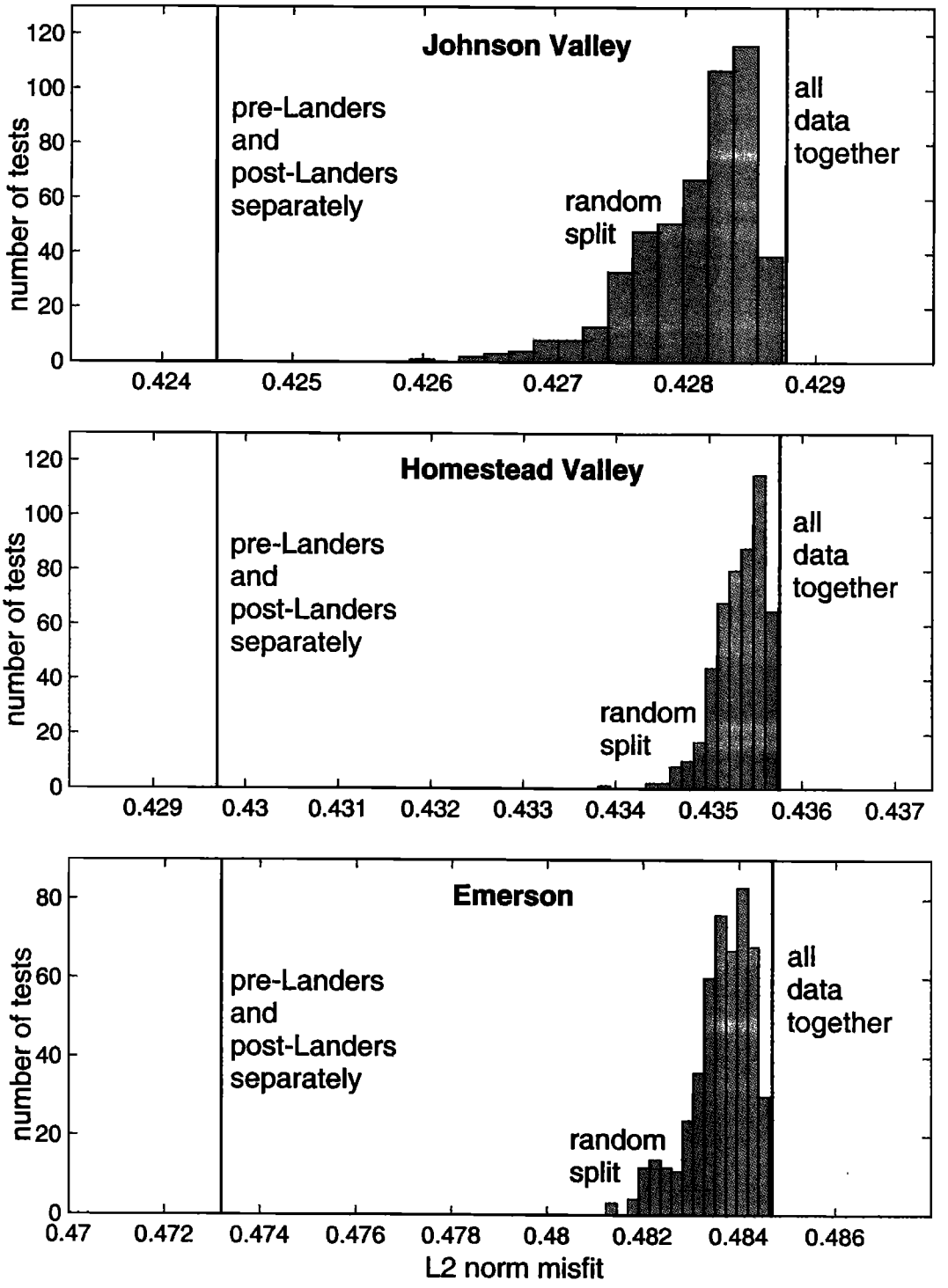

Figure 7. Total misfit of the focal mechanisms of the events occurring along three segments of the Landers rupture (Figure 2) to the best fit stress tensor. The vertical lines represent the misfit if all the events are inverted together and if the premainshock and postmainshock events are inverted separately. The histograms show 500 tests in which the mechanisms were reshuffled and divided into two sets the same sizes at the pre- and post-Landers data sets. The misfit is the L2 norm misfit between the vector of resolved shear stress on the fault plane and a unit vector in the slip direction, which is minimized by the inversion method [*Michael*, 1984, 1987].

field is relatively spatially homogeneous and that the observed premainshock stress orientation is representative of the premainshock stress field in the aftershock zone.

The difference between the pre- and post-Landers stress fields can be demonstrated by showing that a significant reduction in misfit is achieved by inverting the pre- and post-Landers seismicity separately. Figure 7

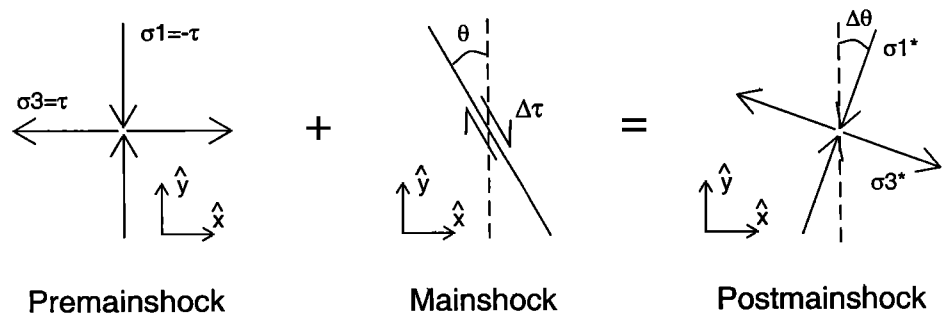

Figure 8. Assumed geometry of a stress rotation due to slip on a fault. The postmainshock stress state is equal to the premainshock stress state plus the stress change due to the earthquake. The problem is assumed to be two-dimensional, so it can be represented entirely in the σ_1-σ_3 plane. θ is the angle from the fault trend to the σ_1 axis, clockwise positive. $\Delta\theta$ is the rotation of the stress field, clockwise positive. The mainshock stress drop, $\Delta\tau$, is taken to be positive for the sense of slip shown and negative for the opposite sense of slip.

shows the total misfit for the events along each segment, with the premainshock and postmainshock data inverted both separately and together. Inverting the two sets separately leads to a misfit reduction, some of which is due to the additional model parameters introduced by inverting for two stress states instead of one. For comparison, the total misfit is also shown for 500 tests in which the mechanisms were reshuffled and divided into two sets the same size as the pre- and post-Landers data sets. The observed misfit reduction is greater than any of the misfit reductions achieved in the tests, implying that the observed misfit reduction cannot be attributed solely to the addition of model parameters. Separate premainshock and postmainshock stress tensors significantly reduce the total misfit, indicating that a difference between the pre- and post-

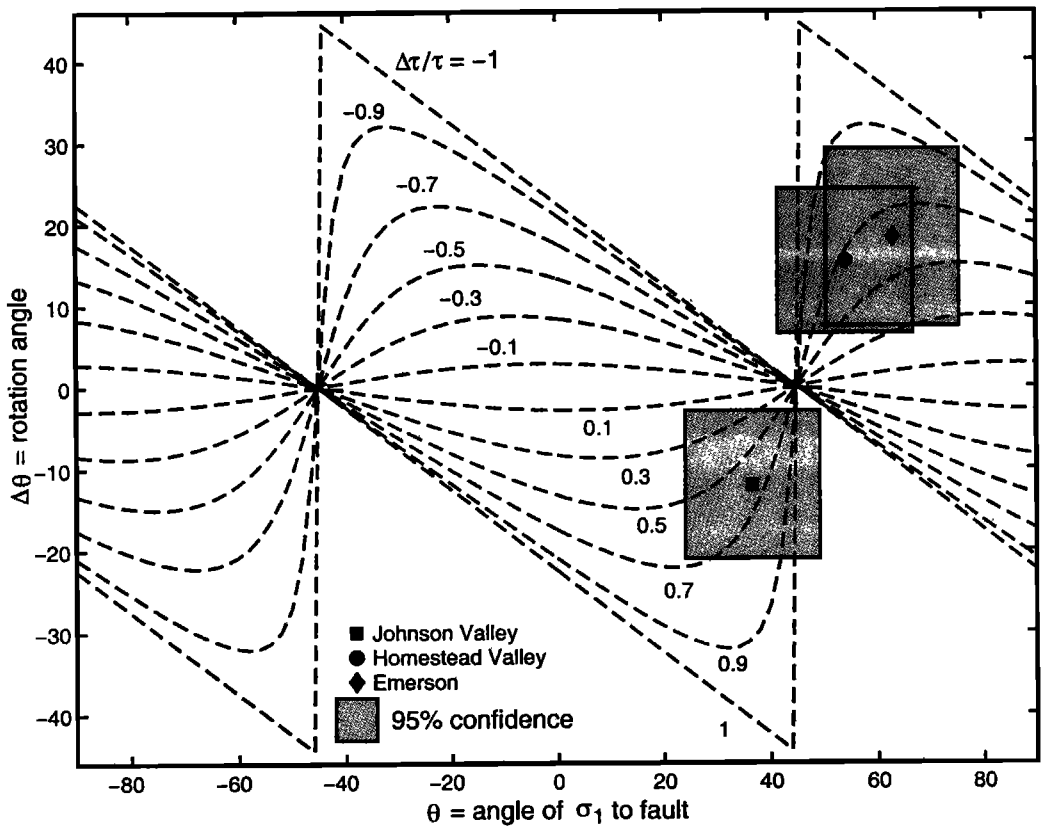

Figure 9. Rotation of the stress field due to an earthquake (equation (4)). The stress rotation, $\Delta\theta$, is shown versus the angle from the fault to the preearthquake σ_1 axis, θ, for various values of $\Delta\tau/\tau$, the ratio of the stress drop to the deviatoric stress magnitude. The geometry is shown in Figure 8. The observed θ and $\Delta\theta$ for three segments of the 1992 Landers earthquake (Figure 2 and Table 1) are shown as solid symbols. Shaded squares are the 95% confidence ranges of the stress orientation and fault strike.

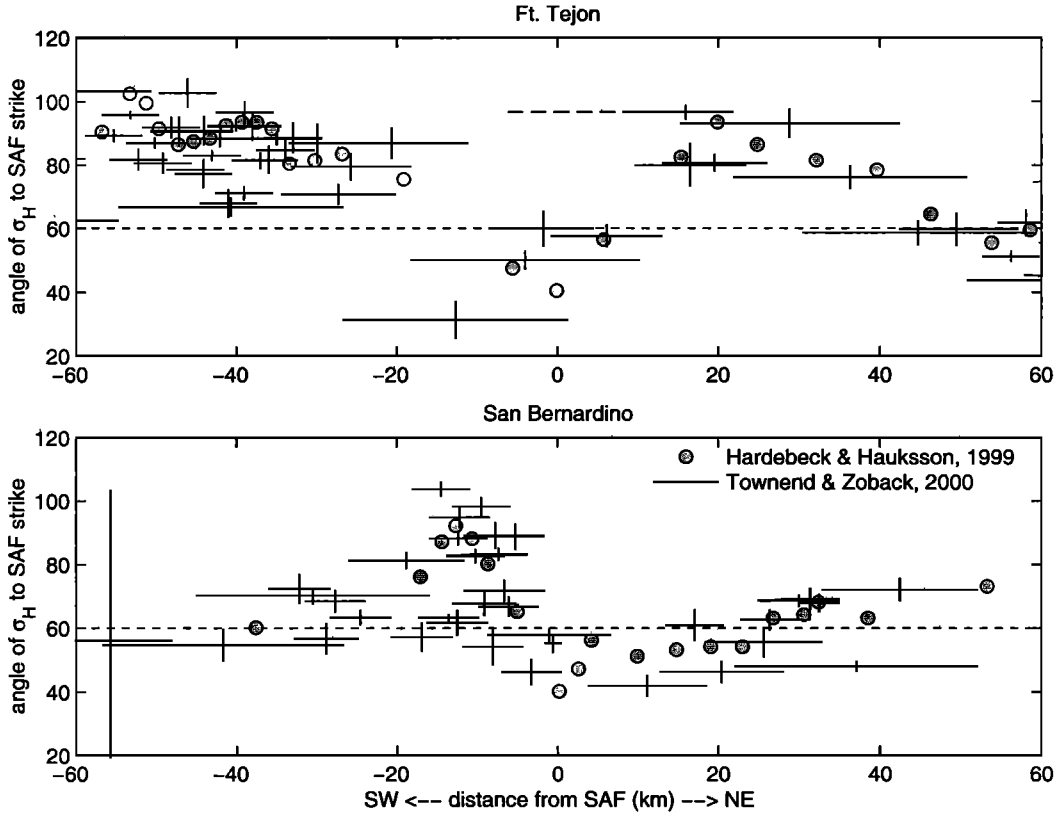

Figure 10. Profiles of σ_H orientation relative to the strike of the San Andreas versus distance from the fault from inversions using two different binning schemes. The circles are adapted from profiles B and D of *Hardebeck and Hauksson* [1999], who binned the events along each profile based on distance from the fault. The solid lines are orientations from *Townend and Zoback* [2000], who used square bins. Each profile shows results from bins located within the approximate along-strike extent of the profiles used by *Hardebeck and Hauksson* [1999]. The lengthes of the horizontal lines represent the spatial extent of the bins in the fault normal direction, and the vertical lines are 1σ error bars (J. Townend, written communication, 2000.) For a bin which crosses the Fort Tejon segment of the fault but contains only events in the opposite corner of the box, the empty portion of the box is indicated with a dashed line. Dashed line at 60° is for reference.

Landers stress states is strongly required by the data.

The magnitude of the deviatoric stress can be estimated quantitatively from the observed 15° (±10°) stress rotation due to Landers. A general 2-D solution can be found for the relationship between the near-field rotation of the stress field and the ratio of the earthquake stress drop, $\Delta\tau$, to the background deviatoric stress magnitude, τ. We follow a procedure similar to that used by *Sonder* [1990] for the stress rotations associated with density anomalies. A solution for earthquake-induced stress changes was previously obtained [*Yin and Rogers*, 1995], but it was based on two assumptions which may not generally hold: that the mainshock fails in accordance with a Coulomb failure criterion and that the magnitude of the deviatoric stress is not changed by the earthquake.

The solution given here assumes that the stress orientation observations are made very near to the mainshock rupture, where the stress change can be approximated by the stress drop. This is a reasonable assumption for most aftershock sequences, in which the majority of events lie along the main rupture. There may be stress and stress drop heterogeneity near the fault due to variable slip, but if the observations represent the uniform part of the stress tensor over the length scale of the rupture and $\Delta\tau$ represents the average stress drop, the result should be the average deviatoric stress on the same length scale.

The postmainshock stress tensor equals the premainshock stress tensor plus the stress change tensor due to the mainshock (Figure 8). The premainshock stress tensor is

$$\sigma_{\mathrm{pre}} = \begin{pmatrix} \tau & 0 \\ 0 & -\tau \end{pmatrix}, \tag{1}$$

where $\tau = (\sigma_3 - \sigma_1)/2$ is the deviatoric stress magnitude and σ_1 and σ_3 are the principal stresses (tension positive). The near-field stress change tensor due to an earthquake on a fault plane oriented at an angle of θ to the σ_1 axis is

$$\Delta\sigma = \begin{pmatrix} -2\Delta\tau\cos\theta\sin\theta & \Delta\tau(\cos^2\theta - \sin^2\theta) \\ \Delta\tau(\cos^2\theta - \sin^2\theta) & 2\Delta\tau\cos\theta\sin\theta \end{pmatrix}, \tag{2}$$

where $\Delta\tau$ is the earthquake stress drop. The postmainshock stress tensor is therefore

$$\sigma_{post} = \sigma_{pre} + \Delta\sigma = \begin{pmatrix} \tau - 2\Delta\tau\cos\theta\sin\theta & \Delta\tau(\cos^2\theta - \sin^2\theta) \\ \Delta\tau(\cos^2\theta - \sin^2\theta) & -\tau + 2\Delta\tau\cos\theta\sin\theta \end{pmatrix}. \quad (3)$$

Solving for the eigenvalues and eigenvectors, one finds that the postearthquake stress tensor is rotated from the preearthquake stress tensor by an angle of $\Delta\theta$, where

$$\Delta\theta = \operatorname{atan}\left(\frac{1-\frac{\Delta\tau}{\tau}\sin 2\theta - \left[\left(\frac{\Delta\tau}{\tau}\right)^2+1-2\frac{\Delta\tau}{\tau}\sin 2\theta\right]^{\frac{1}{2}}}{\frac{\Delta\tau}{\tau}\cos 2\theta}\right). \quad (4)$$

The rotation depends on only two parameters: θ, the orientation of the fault relative to the preearthquake stress field, and $\Delta\tau/\tau$, the ratio of the earthquake stress drop to the background deviatoric stress level. $\Delta\theta$ versus θ is shown for various values of $\Delta\tau/\tau$ in Figure 9.

The ratio $\Delta\tau/\tau$ can be estimated from observed θ and $\Delta\theta$ using this solution. The stress rotations for three segments of the Landers earthquake (Figure 2 and Table 1), shown along with the analytic solution in Figure 9, are used to constrain $\Delta\tau/\tau$. The θ and $\Delta\theta$ observed for the Johnson Valley, Homestead Valley, and Emerson segments are all fit well by a value of $\Delta\tau/\tau$ =0.65. The range of acceptable values for each segment is given in Table 1.

The deviatoric stress magnitude, τ, can be inferred from $\Delta\tau/\tau$ if the earthquake stress drop, $\Delta\tau$, is known. The average stress drop for the Johnson Valley, Homestead Valley, and Emerson segments, estimated from the mapped surface slip, is ~8 MPa (see Table 1). Assuming $\Delta\tau/\tau \approx 0.65$, then $\tau \approx 12$ MPa. This is nearly an order of magnitude less than the crustal strength predicted by laboratory experiments. Conservative error estimates constrain τ to be less than ~25-32 MPa (Table 1). For comparison, the deepest borehole stress measurements in southern California, made at ~3.5 km depth in the Cajon Pass borehole, imply a deviatoric stress magnitude at that depth of ~20±10 MPa [*Zoback and Healy*, 1992].

Laboratory experiments indicate that faults should have a coefficient of friction of 0.6-0.85 [*Byerlee*, 1978], which corresponds to a strength of the order of 100 MPa at seismogenic depths, assuming hydrostatic pore pressure. The active faults in the ECSZ must be weak to operate at shear stress of the order of 10 MPa. Three classes of fault-weakening models have been proposed: high-pressure fluids [*Hubbert and Rubey*, 1959; *Rice*, 1992; *Sibson*, 1992]; inherently weak fault zone materials, although most candidate minerals have been eliminated by laboratory testing [*Moore et al.*, 1996; *Morrow et al.*, 1992]; and dynamic weakening [*Heaton*, 1990; *Melosh*, 1996; *Andrews and Ben-Zion*, 1997; *Harris and Day*, 1997]. These models were formulated to explain the weakness of mature faults with well-developed gouge zones, like the San Andreas, and may need to be modified to apply to lesser developed faults.

The stress orientations obtained from earthquake focal mechanisms represent the uniform part of the stress field on length scales of the order of kilometers or more. Equation (4) relates the rotation of the uniform part of the stress field to the average stress drop on the length scale of the fault. Therefore our observations require low deviatoric stress and low fault strength only on these lengths scales. Smaller-scale variations in fault strength and deviatoric stress magnitude are acceptable and likely. Locally high deviatoric stress magnitudes presumably exist at crack tips and fault irregularities. Dynamic fault weakening mechanisms require small-scale heterogeneity, as locally high shear stress or low static strength is necessary to initiate rupture.

4.4. Mechanics of the San Andreas Fault

The San Andreas Fault is often considered to be a weak fault. The lack of an observed heat flow anomaly along the San Andreas [*Brune et al.*, 1969; *Lachenbruch and Sass*, 1992] indicates that sliding friction is less than ~20 MPa and that the fault is therefore weak in an absolute sense. The San Andreas is also thought to be weak relative to other faults in the region, based on the apparent misorientation of the fault relative to the surrounding stress field. The regional maximum horizontal stress axis, σ_H, has been observed to be roughly perpendicular to the fault surface, indicating that relatively little shear stress is resolved onto the San Andreas compared to faults of other orientations [*Zoback et al.*, 1987; *Mount and Suppe*, 1992]. Since the San Andreas appears to operate at a lower level of shear stress than other faults, it is considered weak in a relative sense.

However, recent work has found that σ_H rotates to lower angles (~50°) near the San Andreas in some parts of southern and central California [*Hardebeck and Hauksson*, 1999; *Provost and Houston*, 2001]. This low angle can be seen in Plate 1 for fault segments with a wide zone of rotation, such as the Tejon Pass segment. Other segments have narrower zones of rotated stress which cannot be well resolved with the 5-20 km spatial resolution of Plate 1. The rotations can be better resolved if the earthquakes are inverted for stress in long narrow bins parallel to the fault.

Townend and Zoback [2000] inverted the same data set as *Hardebeck and Hauksson* [1999] using a different binning technique, and use their observations to argue that σ_H does not rotate to low angle near the fault. However, when their observed stress orientations are displayed as profiles across the San Andreas, it is apparent that these orientations agree very well with those found by *Hardebeck and Hauksson* [1999] (Figure 10). The similarity between the results of the two studies demonstrates that the observed stress rotations across the San Andreas are a robust feature of the focal mechanism data set.

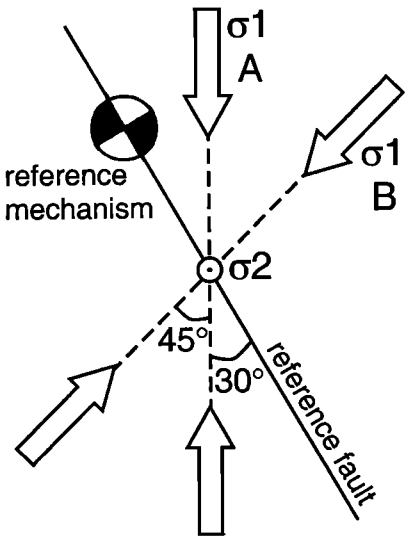

Figure A1. The geometry used to generate the synthetic focal mechanism data sets. The σ_1 axes of stress states A and B are oriented north and N45°E, respectively, and the σ_2 axes are both vertical. The reference fault strikes N30°W, and either stress state would cause this fault to slip in a right-lateral, strike-slip sense, as shown by the reference mechanism. Synthetic focal mechanism data sets are generated by selecting fault planes with different levels of variability from the reference plane and choosing the rake of each event to be in the direction of the resolved shear stress. Random errors can also be added to the data sets. Separate focal mechanism data sets are generated from stress states A and B from the same sets of fault planes.

The observed ~50° angle between σ_H and the fault strike contradicts the model of a relatively weak San Andreas and implies that the shear stress on the fault is approximately equal to the deviatoric stress magnitude in its immediate surroundings. There are two end-member possibilities: that the San Andreas is strong or that the surrounding crust is at low stress. The stress orientation information alone cannot distinguish between these two models.

Scholz [2000] interpreted the stress rotation observed by *Hardebeck and Hauksson* [1999] to mean that the San Andreas is strong. A strong fault driven from below by a shear zone would produce upper crustal stress orientations similar to those observed across the Tejon Pass segment of the San Andreas. However, a strong San Andreas is at odds with heat flow observations [*Lachenbruch and Sass*, 1992].

Hardebeck and Hauksson [1999] interpreted the stress rotation as a ~2-30 km wide zone of weakness due to elevated fluid pressure on the basis of the fault fluid model of *Rice* [1992], which predicts such a rotation. However, as noted by *Scholz* [2000], there is a force balance problem for a wide zone of high fluid pressure, since the model predicts an elevated vertical stress which must be balanced by vertical shear stress on fault-parallel planes. If the zone of high fluid pressure is wide and the deviatoric stress outside of the zone is high, this shear stress is unacceptably large. The model of *Rice* [1992]

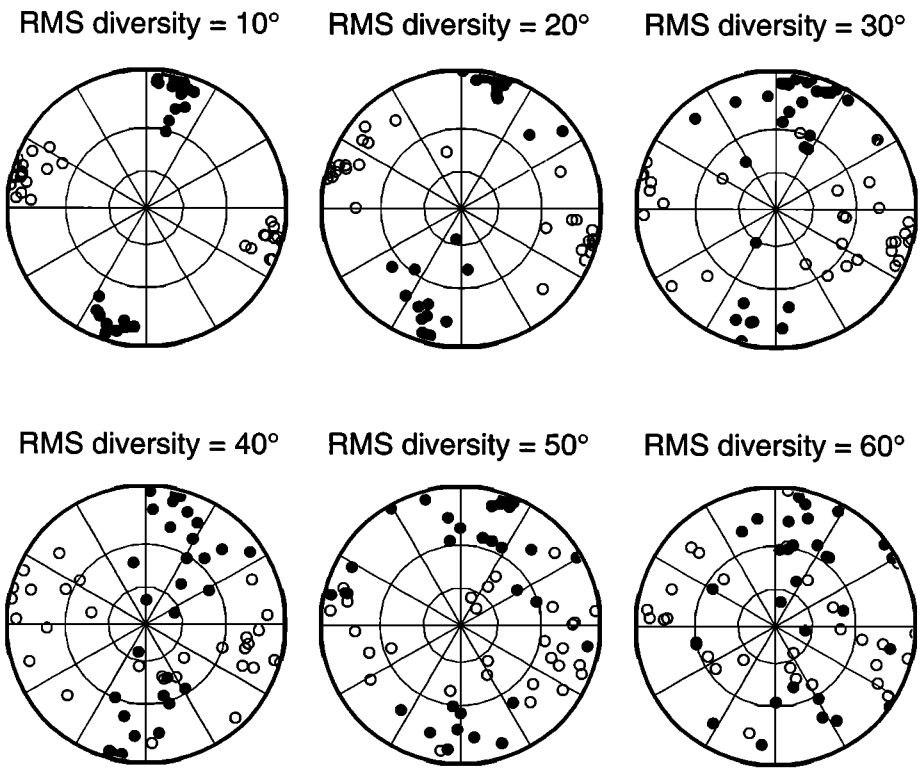

Figure A2. Stereographic projections of the P axes (solid circles) and T axes (open circles) of example focal mechanism data sets illustrating various levels of diversity, as measured by the RMS difference of the mechanisms from the average mechanism. The data sets contain 30 events consistent with stress state A (Figure A1) with the addition of some random errors.

may still apply to the narrow zone of rotation observed in central California [*Provost and Houston*, 2001].

Another possibility is that the San Andreas is a weak fault in a low-stress crust. The low deviatoric stress magnitude observed in the ECSZ suggests that this is the case. If the stress magnitude in the ECSZ is typical of the southern California plate boundary region, the San Andreas may have a resolved shear stress comparable to the deviatoric stress, of the order of 10 MPa, and still be consistent with the upper bound on frictional stress required by heat flow measurements.

The rotation of σ_H across the San Andreas may simply reflect interseismic stress accumulation. If the deviatoric stress is on the order of earthquake stress drop, σ_H should rotate during the seismic cycle, from a high angle immediately following the stress release of a large earthquake to a lower angle later in the interseismic period as the fault is reloaded. The last major earthquake on the San Andreas in southern California was in 1857, so all the fault segments are currently late in the cycle and σ_H is at low angle to the fault. This model predicts the width of the zone of rotation to roughly correspond to the width of the interseismic strain accumulation, which *Hardebeck and Hauksson* [1999] observed.

The observed stress orientations and magnitudes, in southern California and elsewhere, can be explained by a model in which major active faults are weak, while the relatively intact crust is strong. In an intraplate setting, the crust as a whole is strong because it contains no major active faults, and the deviatoric stress is high, as is observed [*Brudy et al.*, 1997]. In a simple plate boundary region, containing only one major active fault, the deviatoric stress magnitude may also be high, but the stress tensor must be oriented such that little shear stress is resolved onto the fault plane. This may be the case for the creeping segment of the San Andreas in central California [*Provost and Houston*, 2001]. In a complex plate boundary region like southern California, however, there are weak faults in many orientations. The crust as a whole cannot support high shear stresses, so the deviatoric stress magnitude must be low.

5. Conclusions

A high-resolution image of stress orientation in the southern California plate boundary region was found from the inversion of earthquake focal mechanisms. The stress field appears to be highly heterogeneous on a range of length scales. Some of the stress field variations can be attributed to the different geologic provinces, fault complexity, and the occurrence of major earthquakes, while some remains unexplained. The complexity of faulting in southern California is not simply the response of a heterogeneous crust to a homogeneous stress state. Fault complexity may lead to stress heterogeneity, and vice versa.

Over the ~20-year time span of the events used in this study, major earthquakes appear to be the dominant cause of temporal evolution of the stress field. In the long term, tectonic loading should approximately cancel out stress changes due to earthquakes. However, since tectonic loading is a much slower process, the stress changes associated with it cannot be confidently observed with ~20 years of earthquake data.

The magnitude of the deviatoric stress can be estimated from the rotation of the stress field caused by major earthquakes. The observed 15° (±10°) stress rotation due to the 1992 Landers earthquake implies that the deviatoric stress is of the order of 10 MPa. This is an order of magnitude less than the fault strength predicted from laboratory experiments, implying that the faults of the Eastern California Shear Zone are weak. This, along with the observation that the San Andreas fault is well oriented for failure in the stress field of its immediate surroundings, suggests that the San Andreas is a weak fault in a low-stress crust.

Appendix A: Quantifying Adequate Focal Mechanism Diversity for Stress Inversion

A single earthquake cannot be used to estimate stress orientation because it requires only that the maximum principal stress axis, σ_1, be in the compressional quadrant of the focal mechanism [*McKenzie*, 1969]. Therefore a set of identical or nearly identical mechanisms

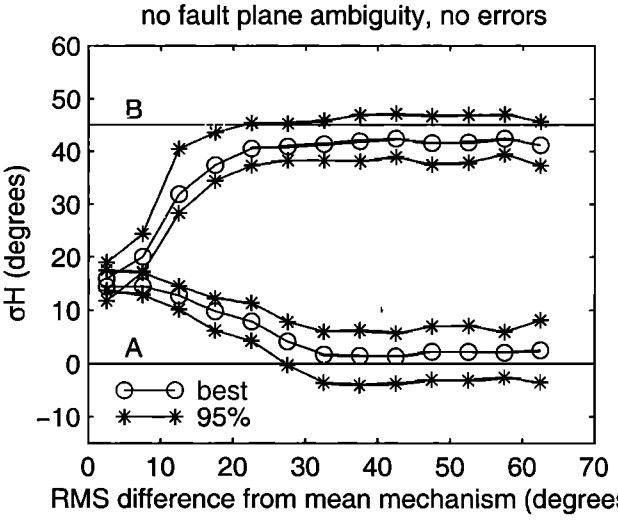

Figure A3. Results of the inversion of perfect synthetic focal mechanism data, with no fault plane ambiguity. The calculated orientation of σ_H is shown versus focal mechanism diversity, as measured by the RMS difference of the mechanisms from the average mechanism, for focal mechanism data sets generated from stress states A and B (see Figure A1). The σ_H orientations for the computed best fit stress states are shown as circles, and the 95% confidence regions are shwon as stars. The horizontal lines at 0° and 45° indicate the correct σ_H orientations for stress states A and B, respectively. Only for data sets with a diversity of at least 30° can the two stress states be correctly recovered.

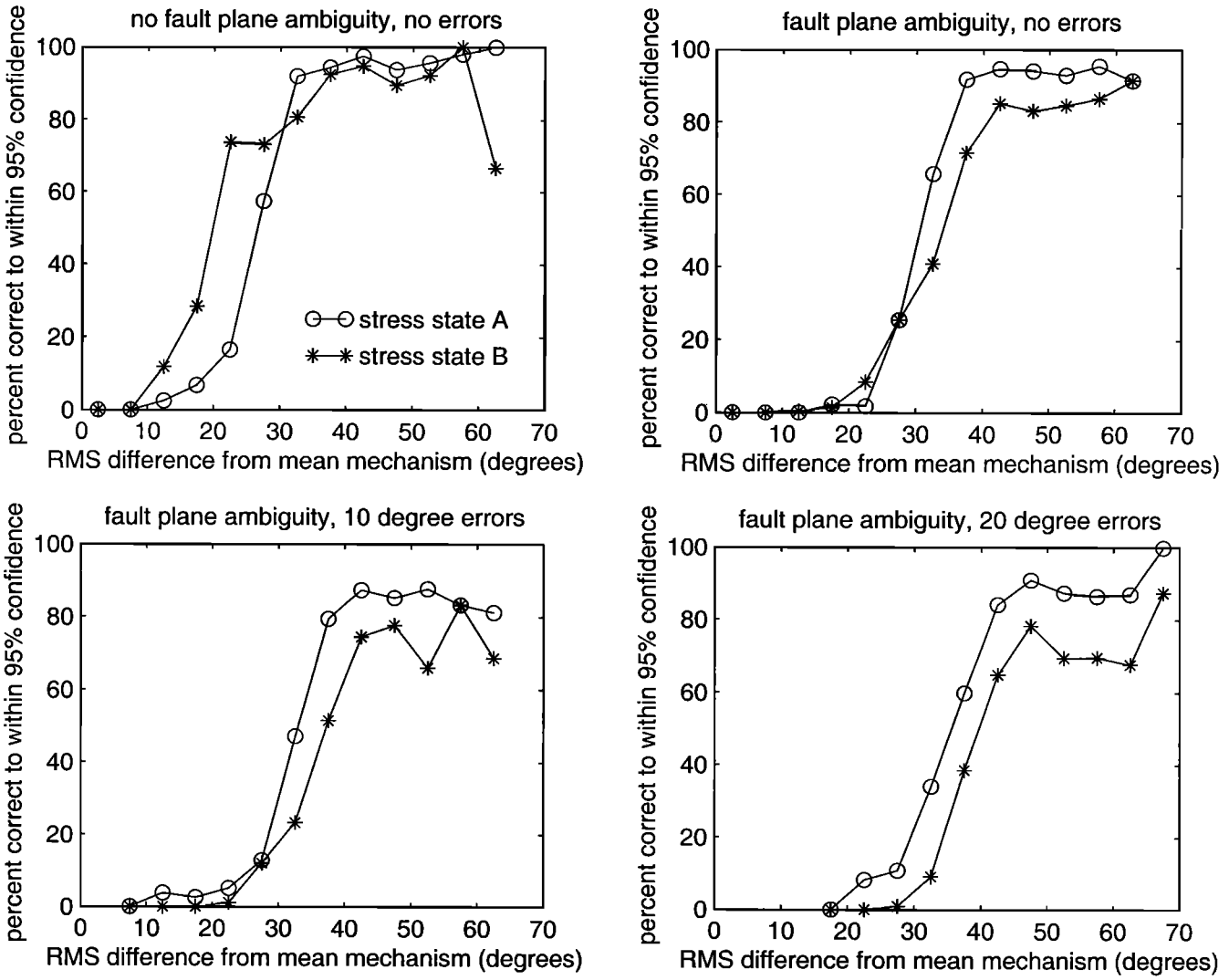

Figure A4. Results from the inversion of ~12,000 synthetic focal mechanism data sets generated from stress states A and B (see Figure A1), with varying numbers of events (30, 50, 100 or 300), level of diversity, and focal mechanism error. The data sets are grouped in 5° bins based on the focal mechanism diversity, as measured by the RMS difference of the mechanisms from the average mechanism. For each bin we plot the percent of data sets for which the correct stress state falls within the computed 95% confidence region. The change from a low percentage to a high percentage indicates the critical level of diversity at which reliable stress inversions become possible.

cannot constrain the stress tensor. An adequately diverse set of fault planes is necessary to obtain a reliable inversion result. However, to our knowledge, no one has quantified how diverse a set of focal mechanisms must be.

We quantify adequate mechanism diversity through a simple test on synthetic data. We select two stress states for which σ_1 is in the same quadrant for a reference focal mechanism and measure how much a focal mechanism data set must vary from the reference mechanism in order to differentiate and correctly recover the two stress states. We generalize the results to propose a simple test which may be used to determine whether a focal mechanism data set is adequately diverse for use in stress inversions.

The geometry for the synthetic tests is shown in Figure A1. For both stress states, σ_2 is vertical. In stress state A, σ_1 trends due north, and for stress state B, σ_1 trends N45°E. The reference fault is vertical and strikes N30°W. Either stress field would cause this fault to slip in a right-lateral, strike-slip sense, as shown by the reference focal mechanism. Earthquakes on more faults of different orientations would clearly be needed to distinguish between the two stress states.

Synthetic focal mechanism data sets are created with varying degrees of diversity. The least diverse sets consist of fault planes which are all very similar to the reference fault plane, while the more diverse sets, although centered about the reference plane, contain more planes of different orientations. The angular difference of the

planes from the reference plane were chosen randomly from a normal, exponential, or flat distribution, with the distribution type having no apparent affect on the results. The focal mechanism data sets for stress state A are found by projecting stress tensor A onto each fault plane and choosing the rake to be in the direction of the resolved shear stress. The synthetic data sets for stress state B are found similarly, for the same sets of fault planes.

Random errors can be introduced into a data set by rotating each mechanism a random angle about a random axis. The angle is chosen from an exponential distribution [*Hardebeck and Hauksson*, 2001], and the rotation axis is chosen from a uniform spatial distribution. Nodal plane ambiguity can be simulated by randomly selecting the fault plane or the auxiliary plane for inclusion in the data set.

For each focal mechanism data set the diversity is quantified by computing an average mechanism and finding the RMS angular difference of the focal mechanisms from this average mechanism. Several other measures of mechanism diversity were also tried, but the RMS angular difference found to be the most diagnostic. Example data sets with varying diversity are shown in Figure A2.

Results for perfect data (no mechanism error and no fault plane ambiguity) are shown in Figure A3. When the mechanism diversity is very low, $\leq 10°$, the inversion results for data generated from stress states A and B are indistinguishable, both with a σ_H direction of ~N15°E, ~45° from the strike of the reference fault. As the diversity increases, the two stress states become more differentiated. For diversity of ~30° or more, both stress states are correctly recovered to within the computed 95% confidence regions.

The results for ~12,000 synthetic data sets are shown in Figure A4. The percent of data sets for which the correct stress state falls within the computed 95% confidence region is plotted versus mechanism diversity. For each level of error, there is a clear critical diversity below which the majority of inversions do not recover the correct stress state and above which they do. The critical diversity is ~30° for perfect data with no fault plane ambiguity and ~35° with the ambiguity. The critical value is ~40° for mechanisms with 10° errors and ~45° for 20° errors.

From this simple synthetic test we have demonstrated that a mechanism diversity of ~40°-45° (for data sets with 10°-20° error) is adequate to differentiate between and correctly recover two stress states which would be indistinguishable with inadequate mechanism diversity. We generalize this result to propose that a given focal mechanism data set is adequately diverse for use in stress inversions if the RMS difference from the average mechanism is greater than ~40°-45°.

Acknowledgments. We thank Andy Michael for providing us with his stress inversion code and for valuable discussions about stress inversion techniques. John Townend and Yukinobi Sugihara kindly shared their stress inversion results. The manuscript was greatly improved by constructive comments from Craig Nicholson and an anonymous reviewer. This work was partially supported by U.S. Geological Survey grant 01HQGR0038 and partially supported by the Southern California Earthquake Center (SCEC), which is funded by NSF Cooperative Agreement EAR-8920136 and USGS Cooperative Agreements 14-08-0001-A0899 and 1434-HQ-97AG01718. SCEC contribution 541. Contribution 8720, Caltech Division of Geological and Planetary Sciences.

References

Abers, G. A., and J. W. Gephart, Stress variations in southern California determined by direct inversion of seismic first motions (MOTSI), *Eos Trans. AGU, 78 (46)* Fall Meet. Suppl., F451, 1997.

Anderson, E. M., *The Dynamics of Faulting and Dyke Formation With Applications to Britain*, Oliver and Boyd, Edinburgh, 1951.

Andrews, D. J., and Y. Ben-Zion, Wrinkle-like slip pulse on a fault between different materials, *J. Geophys. Res., 102*, 552–571, 1997.

Argus, D. F., et al., Shortening and thickening of metropolitan Los Angeles measured and inferred by using geodesy, *Geology, 27*, 703–706, 1999.

Bellier, O., and M. L. Zoback, Recent state of stress change in the Walker Lane zone, western Basin and Range province, United States, *Tectonics, 14*, 5564–5593, 1995.

Brudy, M., M. D. Zoback, K. Fuchs, F. Rummel, and J. Baumgartner, Estimation of the complete stress tensor to 8 km depth in the KTB scientific drill holes: Implications for crustal strength, *J. Geophys. Res., 102*, 18,453–18,475, 1997.

Brune, J. N., T. L. Henyey, and R. F. Roy, Heat flow, stress, and rate of slip along the San Andreas fault, California, *J. Geophys. Res., 74*, 3821–3827, 1969.

Byerlee, J. D., Friction of rock, *Pure Appl. Geophys., 116*, 615–626, 1978.

Castillo, D. A., and M. D. Zoback, Systematic stress variations in the southern San Joaquin Valley and along the White Wolf Fault: Implications for the rupture mechanics of the 1952 M_s 7.8 Kern County earthquake and contemporary seismicity, *J. Geophys. Res., 100*, 6249–6264, 1995.

Dokka, R. K., and C. J. Travis, Late Cenozoic strike-slip faulting in the Mojave Desert, California, *Tectonics, 9*, 311–340, 1990.

Ellsworth, W. L., Earthquake history, 1769-1989, in *The San Andreas fault system, California*, edited by R. E. Wallace, *U. S. Geol. Surv. Prof. Pap.*, 1515, 153-187, 1990.

Hardebeck, J. L., and E. Hauksson, Role of fluids in faulting inferred from stress field signatures, *Science, 285*, 236–239, 1999.

Hardebeck, J. L., and E. Hauksson, Stress orientations obtained from earthquake focal mechanisms: What are appropriate uncertainty estimates?, *Bull. Seismol. Soc. Am., 91*, 250–262, 2001.

Harris, R. A., and S. M. Day, Effects of a low-velocity zone on a dynamic rupture, *Bull. Seismol. Soc. Am., 87*, 1267–1280, 1997.

Hartse, H. E., M. C. Fehler, R. C. Aster, J. S. Scott, and F. L. Vernon, Small-scale stress heterogeneity in the Anza seismic gap, southern California, *J. Geophys. Res., 99*, 6801–6818, 1994.

Hauksson, E., Earthquakes, faulting, and stress in the Los Angeles basin, *J. Geophys. Res., 95*, 15,365–15,394, 1990.

Hauksson, E., State of stress from focal mechanisms before

and after the 1992 Landers earthquake sequence, *Bull. Seismol. Soc. Am.*, *84*, 917–934, 1994.

Hauksson, E., Crustal structure and seismicity distribution adjacent to the Pacific and North America plate boundary in southern California, *J. Geophys. Res.*, *105*, 13,875–13,903, 2000.

Hauksson, E., L. M. Jones, K. Hutton, and D. Eberhart-Phillips, The 1992 Landers earthquake sequence: Seismological observations, *J. Geophys. Res.*, *98*, 19,835–19,858, 1993.

Hauksson, E., L. M. Jones, and K. Hutton, The 1994 Northridge earthquake sequence in California: Seismological and tectonic aspects, *J. Geophys. Res.*, *100*, 12,335–12,355, 1995a.

Hauksson, E., et al., Preliminary report on the 1995 Ridgecrest earthquake sequence in eastern California, *Seismol. Res. Lett.*, *66*, 54–60, 1995b.

Hearn, E. H., and E. D. Humphreys, Kinematics of the southern Walker Lane Belt and motion of the Sierra Nevada block, California, *J. Geophys. Res.*, *103*, 27,033–27,049, 1998.

Heaton, T. H., Evidence for and implications of self-healing pulses of slip in earthquake rupture, *Phys. Earth Planet. Inter.*, *64*, 1–20, 1990.

Hickman, S. H., M. D. Zoback, and J. H. Healy, Continuation of a deep borehole stress measurement profile near the San Andreas Fault, 1, hydraulic fracturing stress measurements at Hi Vista, Mojave Desert, California, *J. Geophys. Res.*, *93*, 15,183-15,195, 1988.

Horiuchi, S., G. Rocco, and A. Hasegawa, Discrimination of fault planes from auxiliary planes based on simultaneous determination of stress tensor and a large number of fault plane solutions, *J. Geophys. Res.*, *100*, 8327–8338, 1995.

Hubbert, M. K., and W. W. Rubey, Mechanics of fluid-filled porous solids and its application to overthrust faulting, part 1, role of fluid pressure in mechanics of overthrust faulting, *Geol. Soc. Am. Bull.*, *70*, 115–166, 1959.

Jennings, P., Fault map of California with volcanoes, thermal springs and thermal wells, scale 1:750,000, in *Geol. Data Map 1*, Calif. Div. of Mines and Geol., Sacramento, 1975.

Johnson, H. O., D. C. Agnew, and F. K. Wyatt, Present-day crustal deformation in southern California, *J. Geophys. Res.*, *99*, 23,951–23,974, 1994.

Jones, L. M., Focal mechanisms and the state of stress on the San Andreas Fault in southern California, *J. Geophys. Res.*, *93*, 8869–8891, 1988.

Kerkela, S., and J. M. Stock, Compression directions north of the San Fernando Valley determined from borehole breakouts, *Geophys. Res. Lett.*, *23*, 3365–3368, 1996.

King, N. E., and W. Thatcher, The coseismic slip distribution of the 1940 and 1979 Imperial Valley, California, earthquakes and their implications, *J. Geophys. Res.*, *103*, 18,069–18,086, 1998.

Lachenbruch, A. H., and J. H. Sass, Heat flow from Cajon Pass, fault strength, and tectonic implications, *J. Geophys. Res.*, *97*, 4995–5015, 1992.

Liu, Y., S. Crampin, and R. E. Abercrombie, Shear-wave anisotropy and the stress field from borehole recordings at 2.5 km depth at Cajon Pass, *Geophys. J. Int.*, *129*, 439–449, 1997.

McKenzie, D. P., The relation between fault plane solutions for earthquakes and the directions of the principal stresses, *Bull. Seismol. Soc. Am.*, *59*, 591–601, 1969.

Melosh, H. J., Dynamical weakening of faults by acoustic fluidization, *Nature*, *379*, 601–606, 1996.

Michael, A. J., Determination of stress from slip data: Faults and folds, *J. Geophys. Res.*, *89*, 11,517–11,526, 1984.

Michael, A. J., Stress rotation during the Coalinga aftershock sequence, *J. Geophys. Res.*, *92*, 7963–7979, 1987.

Michael, A. J., Spatial variations in stress within the 1987 Whittier Narrows, California, aftershock sequence: New techniques and results, *J. Geophys. Res.*, *96*, 6303–6319, 1991.

Moore, D. E., D. A. Lockner, R. Summers, S. Ma, and J. D. Byerlee, Strength of chrysotile-serpentinite gouge under hydrothermal conditions: Can it explain a weak San Andreas Fault?, *Geology*, *24*, 1041–1044, 1996.

Morrow, C., B. Radney, and J. Byerlee, Frictional strength and the effective pressure law of montmorillonite and illite clays, in *Fault Mechanics and Transport Properties of Rock*, edited by B. Evans and T.-F. Wong, pp. 69–88, Academic, San Diego, Calif., 1992.

Mount, V. S., and J. Suppe, Present-day stress orientations adjacent to active strike-slip faults; California and Sumatra, *J. Geophys. Res.*, *97*, 11,995–12,013, 1992.

Nur, A., H. Ron, and G. C. Beroza, The nature of the Landers-Mojave earthquake line, *Science*, *261*, 201–203, 1993.

Provost, A.-S., and H. Houston, Orientation of the stress field surrounding the creeping section of the San Andreas fault: Evidence for a narrow mechanically-weak fault zone, *J. Geophys. Res.*, *106*, 11,373–11,386, 2001.

Reasenberg, P., and D. Oppenheimer, FPFIT, FPPLOT and FPPAGE: FORTRAN computer programs for calculating and displaying earthquake fault-plane solutions, *U.S. Geol. Surv. Open File Rep.*, *85-730*, 109, 1985.

Rice, J. R., Fault stress states, pore pressure distributions, and the weakness of the San Andreas Fault, in *Fault Mechanics and Transport Properties of Rock*, edited by B. Evans and T.-F. Wong, pp. 475–503, Academic, San Diego, Calif., 1992.

Richards-Dinger, K. B., and P. M. Shearer, Earthquake locations in southern California obtained using source-specific station terms, *J. Geophys. Res.*, *105*, 10,939–10,960, 2000.

Saucier, F., E. Humphreys, and R. Weldon, Stress near geometrically complex strike-slip faults: Application to the San Andreas Fault at Cajon Pass, southern California, *J. Geophys. Res.*, *97*, 5081–5094, 1992.

Scholz, C. H., Evidence for a strong San Andreas Fault, *Geology*, *28*, 163–166, 2000.

Shamir, G., and M. D. Zoback, Stress orientation profile to 3.5 km depth near the San Andreas Fault at Cajon Pass, California, *J. Geophys. Res.*, *97*, 5059–5080, 1992.

Sibson, R. H., Implications of fault-valve behaviour for rupture nucleation and recurrence, *Tectonophysics*, *211*, 283–293, 1992.

Sieh, K., et al., Near-field investigation of the Landers earthquake sequence, April to July 1992, *Science*, *260*, 171–176, 1993.

Simpson, R. W., Quantifying Anderson's fault types, *J. Geophys. Res.*, *102*, 17,909–17,919, 1997.

Sonder, L. J., Effects of density contrasts on the orientation of stresses in the lithosphere: Relation to principal stress directions in the Transverse Ranges, California, *Tectonics*, *9*, 761–771, 1990.

Stock, J. M., and J. H. Healy, Conitnuation of a deep borehole stress measurement profile near the San Andreas Fault, 2, Hydraulic fracturing stress measurements at Black Butte, Mojave Desert, California, *J. Geophys. Res.*, *93*, 15,196–15,206, 1988.

Townend, J., and M. D. Zoback, Implications of earthquake focal mechanisms for the frictional strength of the San Andreas Fault system, paper presented at Geological Society of London Conference on Weak Faults, London, UK, 2000.

Wald, D. J., D. V. Helmberger, and S. H. Hartzell, Rupture

process of the 1987 Superstition Hills earthquake from the inversion of strong-motion data, *Bull. Seismol. Soc. Am.*, *80*, 1079–1098, 1990.

Walls, C., T. Rockwell, K. Mueller, Y. Bock, S. Williams, J. Pfanner, J. Dolan, and P. Fang, Escape tectonics in the Los Angeles metropolitan region and implications for seismic risk, *Nature*, *394*, 356–360, 1998.

Weldon, R. J., and J. E. Springer, Active faulting near the Cajon Pass well, southern California: Implications for the stress orientations near the San Andreas Fault, *Geophys. Res. Lett.*, *15*, 993–996, 1988.

Wilde, M., and J. Stock, Compression directions in southern California (from Santa Barbara to Los Angeles Basin) obtained from borehole breakouts, *J. Geophys. Res.*, *102*, 4969–4983, 1997.

Wyss, M., and Z. Lu, Plate boundary segmentation by stress directions: Southern San Andreas fault, California, *Geophys. Res. Lett.*, *22*, 547–550, 1995.

Yin, Z.-M., and G. C. Rogers, Rotation of the principal stress directions due to earthquake faulting and its seismological implications, *Bull. Seismol. Soc. Am.*, *85*, 1513–1517, 1995.

Zhao, D., and H. Kanamori, The 1994 Northridge earthquake: 3-D crustal structure in the rupture zone and its relation to the aftershock locations and mechanisms, *Geophys. Res. Lett.*, *22*, 763–766, 1995.

Zhao, D., H. Kanamori, and D. Wiens, State of stress before and after the 1994 Northridge earthquake, *Geophys. Res. Lett.*, *24*, 519–522, 1997.

Zoback, M. D., and J. H. Healy, In situ stress measurements to 3.5 km depth in the Cajon Pass scientific research borehole: Implications of the mechanics of crustal faulting, *J. Geophys. Res.*, *97*, 5039–5057, 1992.

Zoback, M. D., et al., New evidence on the state of stress of the San Andreas Fault system, *Science*, *238*, 1105–1111, 1987.

Zoback, M. L., First- and second-order patterns of stress in the lithosphere: The World Stress Map project, *J. Geophys. Res.*, *97* , 11,703–11,728, 1992.

J. L. Hardebeck, Institute of Geophysics and Planetary Physics, Scripps Institution of Oceanography, University of California, San Diego, La Jolla, CA 92093-0225, USA.

E. Hauksson, Seismological Laboratory MC 252-21, California Institute of Technology, Pasadena, CA 91125, USA.

(Received September 28, 2000; revised March 9, 2001; accepted April 4, 2001.)